CHALMERS
UNIVERSITY OF TECHNOLOGY

Joint Detection and Localization with an Efficient Censoring Method for Distributed Monopulse Radars under Communication Constraints

Citation for the original published paper (version of record):
Lai, Y., Yang, S., Keskin, M. et al (2025). Joint Detection and Localization with an Efficient Censoring Method for Distributed Monopulse
Radars under Communication Constraints. IEEE Transactions on Aerospace and Electronic Systems, 61(5): 12702-12724. http://dx.doi.org/10.1109/TAES.2025.3575059

(article starts on next page)

Joint Detection and Localization with an Efficient Censoring Method for Distributed Monopulse Radars under Communication Constraints

Yangming Lai, *Member, IEEE*, Shixing Yang, *Member, IEEE*, Musa Furkan Keskin, *Member, IEEE*, Henk Wymeersch, *Fellow, IEEE*, Lingjiang Kong, *Senior Member, IEEE* and Wei Yi, *Senior Member, IEEE*

***Abstract*—This paper deals with the joint detection and localization (JDL) problem in distributed monopulse radars considering communication constraints. Initially, we devise a JDL algorithm with unlimited communication rates (JDL-UCR) to realize multi-target detection and localization by directly utilizing raw sampled signals at the fusion center (FC). Theoretically, joint processing of raw data yields superior detection and/or localization performance in distributed radars. However, the extensive data transmission bandwidth required between each local station and the FC is unfeasible, especially in wireless communication-constrained environments. To tackle this challenge, leveraging the theoretical groundwork of the JDL-UCR, we further propose a JDL algorithm with an efficient censoring method (JDL-ECM). In this algorithm, we formulate a regular censoring rule and derive both closed-form and adaptive censoring threshold expressions to effectively exclude the non-essential data of each local station. Additionally, we establish a three-step data updating operation to effectively retain the informative data including moving targets as much as possible. Consequently, the proposed JDL-ECM focuses on alleviating the data communication burden while maintaining superior detection and localization performance. Finally, we provide a comprehensive performance analysis, employing both simulation and real experimental data, to demonstrate the effectiveness of the proposed JDL-ECM algorithm. The analysis showcases its capability to achieve accurate detection and localization results under stringent communication constraints.**

***Index Terms*—Joint detection and localization, distributed radars, communication constraints, censoring.**

The work of Yangming Lai, Lingjiang Kong, and Wei Yi was supported in part by the scholarship from China Scholarship Council (CSC) under Grant No. 202206070041, and in part by the National Natural Science Foundation of China under Grants 62231008. The work of Shixing Yang was supported by the Fundamental Research Funds for the Central Universities under Grant XJSJ25003. The work of Musa Furkan Keskin and Henk Wymeersch was supported in part by the SNS JU project 6G-DISAC under the EU's Horizon Europe research and innovation Program under Grant Agreement No 101139130, and in part by the Swedish Research Council (VR) through the project 6G-PERCEF under Grant 2024-04390. (*Corresponding author: Wei Yi.*)

Yangming Lai, Lingjiang Kong and Wei Yi are with the School of Information and Communication Engineering, University of Electronic Science and Technology of China, Chengdu 611731, China (e-mail: ymlai1996@gmail.com; ljkong@uestc.edu.cn; kussoyi@gmail.com).

Shixing Yang is with the National Key Laboratory of Radar Signal Processing, Xidian University, Xi'an 710071, China (e-mail: victorshixing@gmail.com).

Musa Furkan Keskin and Henk Wymeersch are with the Department of Electrical Engineering, Chalmers University of Technology, 41296, Gothenburg, Sweden (email: furkan@chalmers.se; henkw@chalmers.se).

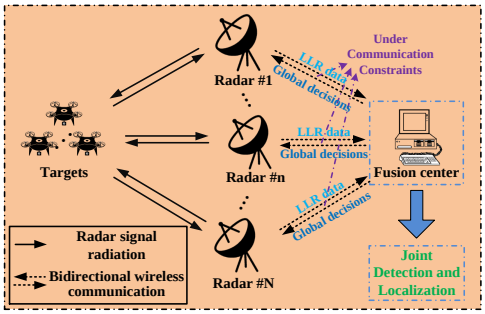

Figure 1. Illustration of the distributed radars. We can see multiple targets are surveilled by multiple radars through radiating electromagnetic waves, and a fusion center (FC) communicates with the radars by bidirectional wireless communication links under communication constraints. The FC will make full use of the transmitted local log-likelihood ratio (LLR) data to implement the JDL of targets and feed the global decisions back to the local stations.

I. Introduction

A. Background and Motivation

Recent advances in radar technology have spurred considerable interest in distributed radar systems [1]–[4]. These systems are being explored extensively for applications in the civilian domain, including surveillance security [5], automotive assistance/automated driving [6], and human activity recognition [7]. Compared with a single radar, distributed radars have a wider field of view to observe targets from different angles. The resulting spatial and geometric diversity can be leveraged to mitigate the scintillation of the radar cross section (RCS) [8], [9], thus raising the performance of target imaging [10], detection [11], [12], localization [13], [14], and tracking [15]–[17].

Generally speaking, there are two main approaches to realize target detection and/or localization in distributed radars. The first approach is the two-step technique: firstly, preliminary detection and estimation are performed at each local station; then the obtained local decisions '0/1' and estimated position measurements like the angle of arrival (AOA) [18] and time of arrival (TOA) [19] are transmitted to a fusion center (FC) [20]; finally, the FC realizes the global detection by employing 'AND', 'OR', or 'M out of N' rules [21] and localization via the pairing and triangulation of the extracted parameters [22]. This approach requires a relatively low computational burden and transmission bandwidth between local stations and the FC. However, the corresponding performance

may drop significantly because of the simplified extraction of raw data information, especially the occurrence of missed detections and/or estimation errors at some local stations.

The second approach directly and jointly processes the local raw observations (i.e., like the raw baseband echoes or likelihood values observed by each local station) at the FC for target separate detection [23]–[26], separate (direct) localization [27]–[32], and joint detection and localization (JDL) [33]–[39]. Separate detection research mainly focuses on investigating detection performance on a single grid. Direct localization achieves localization without detection by utilizing maximum likelihood (ML) estimation of the target's location within an inspected region that encompasses many grids. Meanwhile, JDL research is dedicated to implementing simultaneous detection and localization of targets, whose actions are also undertaken on location grids of an inspected region. Technically, these approaches make full use of received signal information for detection and/or localization without the need for local decision fusion or target-measurement association, as in the former two-step approach. It also results in more robust detection and/or localization performance, especially in low signal-to-noise ratio (SNR) scenarios. However, it is not practical to transmit the large amount of data from each local node to the FC especially when the communication constraints are considered. Therefore, signal processing methods based on low communication burden are imperative. The current works that meet the aforementioned requirement can be classified into three categories, as outlined in the following:

- The first category is related to the applications of *compressed sensing (CS)* for distributed radar systems [38], [40]–[42], which aims to accurately reconstruct data from significantly fewer samples than the Nyquist rate. It is demonstrated that both the sparse modeling [40] and recovery techniques [41] can reduce the amount of data samples for direct localization, respectively. A distributed CS based joint detection and tracking algorithm is presented in [42]. Besides, [38] proposes a CS based framework to realize the enumeration and localization of targets under a lower communication load.
- The second category is the *data quantization* methods [31], [43]–[46] that measure the raw baseband echoes or likelihood values of local stations at a lower bit depth. The study of [43] consider the quantization-based detection in bandwidth-constraint wireless sensor networks. The works in [44] and [45] investigate the multi- and one-bit detection for multiple-input multiple-output (MIMO) radars, respectively. In [31], a low-bit direct localization algorithm is proposed by employing ML estimation. Additionally, [46] introduces the implementation of hybrid quantized detection within distributed radar systems.
- Differing from the former two categories, the third category is related to *censoring strategies* that only transmit a part of local observations to the FC for data fusion [47]–[53]. The studies in [47], [48] show that for conditionally independent sensor data, transmission occurs only when the local log-likelihood ratio (LLR) exceeds the 'no-send' interval boundaries, as supported by both Neyman–Pearson and Bayesian frameworks. Spatial dependence among sensor data [49] and uncertainty noise power [50] are considered in the distributed detection for censoring sensor networks. Two-stage constant false alarm rate (CFAR) detectors based on censoring method are investigated in [51] for distributed radar systems. The research in [52] also employs censored observations to realize decentralised detection in multistatic radar. Besides, the censoring strategy is applied by [53] to realize the distributed detection of sparse signals in energy-limited clustered sensor networks.

These categories require processing raw observations or likelihood values at each radar before data transmission. Note that in the delay-dimensional data, after matched filtering or LLR calculation, many delay bins are noisy and target-free. Under low data transmission requirements in distributed radars, particularly with communication constraints, censoring becomes crucial. This approach focuses on censoring most non-essential data while retaining informative data, including target information, which is a key focus of our study. Moreover, the presence of multiple targets with varying RCS sizes presents additional challenges for the application of censoring methods. Specifically, weak targets may be adversely affected by stronger ones, leading to misdetection in low-SNR scenarios and performance degradation. Thus, a nuanced censoring approach is necessary. In this study, we aim to develop an efficient censoring method that enhances the informativeness of limited transmission data, thereby enabling high-performance detection and localization of multiple moving targets with stringent communication constraints. To the best of our knowledge, the problem of minimizing data transmission through a *censoring strategy incorporating feedback from the FC to local radars* in the context of *multi-target* JDL within *distributed radar systems* has not yet been addressed in the existing JDL literature.

B. Main Contributions

Based on the above research background and motivation, this paper investigates the JDL problem in practical distributed monopulse radars under communication constraints. We first devise an algorithm to realize the JDL of multiple targets with unlimited communication rates. Building upon this theoretical foundation, we further propose another algorithm tailored for the communication-constrained environments. Finally, we verify the effectiveness of our proposed procedures by the simulated and real experimental data with practical frequency-modulated continuous wave (FMCW) waveforms. More specifically, the main contributions can be summarized as follows.

1) *We devise the JDL with unlimited communication rates (JDL-UCR) algorithm.* Upon formulating the JDL problem as a composite multiple hypotheses test directly applied to the raw sampled signals, we first elaborate on a multi-target generalized likelihood ratio test (GLRT) detector which can realize the simultaneous detection and localization of multiple targets. However, it is computationally demanding in practical applications as it requires

prohibitive high-order search. Then, a low-dimensional solution is employed to simplify the high-order search problem to a series of two-dimensional search problems. Next, the complete obtained LLR values of the local radars are transmitted to the FC for global decision, assuming the communication-rate upper bound between the local stations and FC is unlimited. Finally, the targets will be extracted one by one, thus realizing the JDL of multiple targets with unlimited communication rates.

2) *We then propose the JDL algorithm with an efficient censoring method (JDL-ECM) under communication constraints.* Considering the specific limited communication rates between each local station and the FC, we formulate a regular censoring rule and derive both closed-form and adaptive censoring threshold expressions to filter out most parts of the LLR values and retain relatively informative data. Then, we establish a three-step data updating operation. The first step employs the previous-frame global estimated locations and velocities of targets (if detected), which were fed back from the FC to local stations, to make location predictions and extract parts of the current original LLR data. Besides, two steps containing transmission space freeing and data vectors combining are designed to produce an updated informative LLR data vector while avoiding the data transmission exceeding the communication constraints. Finally, the updated vectors are transmitted to the FC and a new global decision rule is designed for the iterative detection and localization of multiple targets.
3) *We provide a comprehensive performance analysis conducted using both simulation and real experimental data to verify the effectiveness of our proposed procedures.* On the one hand, we provide simulation analysis including the detection and localization performance analyses under both the single and multiple moving targets cases. Simulation results show that the proposed JDL-ECM, which operates under stringent communication constraints, can achieve performance close to that of JDL-UCR without any communication constraints. On the other hand, two real experimental scenarios, one involving a strong or a weak target and the other involving two targets, are designed to demonstrate the feasibility of the proposed algorithm in practical operations. The analyses also reveal that the performance of the proposed algorithm is particularly robust, especially in low-SNR cases.

The main distinctive differences between this paper and recent works on communication constraints in distributed radars are summarized in Table I. The results clearly demonstrate the advantages of this work in addressing the practical demands of detecting and localizing multiple moving targets for distributed monopulse radars under communication constraints.

Besides, the closest related works include [35], [36], [39]. Significant differences exist in the employed models, considered problems, and employed techniques, as summarized in Table II. Specifically, [35] investigates the JDL problem of multiple stationary targets in distributed monopulse radar systems, while [36] develops subspace-based JDL algorithms to mitigate sidelobes masking effects in these systems. The work [39] investigates the JDL problem of multiple moving targets in distributed multi-pulse radars. These works assume that radars transmit complete received baseband signals [35], [36] or delay-Doppler LLR data [39] to the FC *without considering any communication constraints*. In contrast, this paper centers on designing an efficient censoring framework that maintains high detection and localization performance of multiple moving targets *under stringent communication constraints*. It should be noted that, the key contribution of this work is not the detailed implementation of JDL of multiple moving targets, but to design an efficient censoring method to decrease the transmitted data amount as much as possible when the strong communication constraints between the FC and the radars are considered, while enabling consistent high detection and localization performance compared with the case of no communication constraints. In Table II, it can be seen that the works [36], [39], and this paper investigate different problems which were not solved in [35]. To solve the communication-constraint problem, designing an efficient censoring method in this paper offers sufficient novelty and is not covered in the closest related works.

Table I
COMPARISON BETWEEN THIS PAPER AND RECENT WORKS ON COMMUNICATION CONSTRAINTS IN DISTRIBUTED RADAR SYSTEMS

Ref.	Detection	Localization	Moving Target	Multiple Targets	Method
[40], [41]	✗	✓	✓	✓	CS
[38]	✗	✓	✗	✓	CS
[44], [46]	✓	✗	✓, ✗	✗	Quantization
[31]	✗	✓	✗	✗	Quantization
[51], [52]	✓	✗	✗	✗	Censoring
This Paper	✓	✓	✓	✓	Censoring

The remainder of this paper is organized as follows[1]. In Section II, we present the system and signal model. Section III devised the JDL-UCR algorithm and computes the high communication rates between each local radar and FC. Section IV describes the proposed JDL-ECM algorithm. Section V presents the performance assessment including simulation analysis and experimental tests. Finally, the conclusions of the whole paper are provided in Section VI.

II. SYSTEM AND SIGNAL MODEL

As illustrated in Fig. 1, we consider a distributed radar system with N local stations located at $\{\boldsymbol{x}_n\}_{n=1}^{N} \in \mathbb{R}^2$ and P point-like targets [54] initially located at $\boldsymbol{\theta}_p \in \mathbb{R}^2$ with velocity $\boldsymbol{v}_p \in \mathbb{R}^2$ ($p = 1, \ldots, P$, where P is an apriori

[1]Lowercase boldface letters are used to denote column vectors, while uppercase boldface letters denote matrices. The operations of conjugation, transposition, and conjugate-transposition are represented by $(\cdot)^*$, $(\cdot)^{\top}$, and $(\cdot)^H$, respectively. The notation cat$\{\boldsymbol{a}_1, \ldots, \boldsymbol{a}_Y\}$ is used to form an MY-dimensional vector by concatenating the M-dimensional vectors $\{\boldsymbol{a}_n\}_{n=1}^{Y}$. The $M \times M$ identity matrix is denoted as $\mathbf{I}_M$. The symbols $\jmath$, $\otimes$, and $+$ stand for the imaginary unit, the Kronecker product, and the pseudoinverse operator, respectively. Finally, $\lceil \cdot \rceil$, $\| \cdot \|$, $\mathbb{E}\{\cdot\}$, and $\delta(\cdot)$ represent the ceiling function, Euclidean norm, statistical expectation, and impulse function, respectively.

Table II
COMPARISON BETWEEN THIS PAPER AND THE CLOSEST RELATED WORKS

Features	Ref. [35]	Ref. [36]	Ref. [39]	This Paper
Signal Model	Monopulse	Monopulse	**Multi-Pulse**	Monopulse
The Mobility of Multiple Targets	Stationary	Stationary	**Moving**	**Moving**
Sidelobe Masking Effects	Omitted	**Considered**	Omitted	Omitted
Grid Search	Location Region	Location Region	**Location and Velocity Region**	Location Region
Communication Constraints	Omitted	Omitted	Omitted	**Considered**

unknown variable)[2]. It is supposed that the stations share a common time reference[3], employ different carrier frequencies $\{f_c^n\}_{n=1}^N$ to avoid mutual interference [56], and can observe all targets in the common viewing area. An FC communicates with each station by bidirectional wireless links (e.g., standard half-duplex communication) which are considered to be rates-limited under communication constraints without any other influences. Besides, the calibration problems (e.g., mutual coupling, phase mismatches) of radar antennas are assumed to be perfectly solved in this system.

A. Transmit Signal

Firstly, we assume that the waveforms $\{x_n(t)\}_{n=1}^N$ with a bandwidth B are time-limited to $[0, T]$, satisfying the property $f_{\max} T \ll 1$, where T is the modulated duration and $f_{\max} \geq 0$ is the maximum magnitude of the Doppler shift in any target echo. This property implies that the Doppler shifts in the received echoes can be neglected, which is also the typical case observed over a single pulse repetition interval (PRI) in pulse radars [28], [36], [38], [57]. The waveforms are assumed to have thumbtack auto-correlation functions [31], [35] and be approximately orthogonal between each other for the time delay τ of interest[4] [28], such that

$$\int_T x_n(t) x_{n'}^*(t-\tau)\, dt \approx 0, n \neq n'. \tag{1}$$

Then, the complex baseband transmit signal of the n-th station is denoted by

$$\tilde{s}_n(t) = \sqrt{E/N} x_n(t) W(t) \tag{2}$$

where $0 < t \leq T_{\text{pri}}$, T_{pri} is the duration of a PRI, and E represents the total transmitted energy; $W(t)$ is a rectangular window, i.e.,

$$W(t) = \begin{cases} 1, & 0 < t \leq T_{\text{pri}} \\ 0, & \text{otherwise.} \end{cases} \tag{3}$$

We assume that the duration of one frame T_{frame} includes one PRI and also allocates an idle duration T_{idle} for data processing and transmission, i.e., $T_{\text{frame}} = T_{\text{pri}} + T_{\text{idle}}$. The baseband transmit signal is first generated and then undergoes upconversion, where it is mixed with a local oscillator signal to modulate it to a higher radio frequency (RF) carrier frequency f_c^n. Therefore, the transmitted signal of the n-th station can be written as $\Re\left\{\tilde{s}_n(t) e^{\jmath 2\pi f_c^n t}\right\}$.

B. Continuous-time Received Signal

The received signal, which was reflected upon P targets, observed, downconverted and quadrature demodulation by the n-th station, can be represented as

$$\tilde{r}_n(t) = \sum_{p=1}^{P} \tilde{\alpha}_{n,p} \tilde{s}_n\left(t - \tau_{n,p}\right) e^{-\jmath 2\pi f_c^n \tau_{n,p}} + \tilde{w}_n(t) \tag{4}$$

where $\tilde{\alpha}_{n,p}$ is the complex reflection coefficient, the time delay $\tau_{n,p}$ can be calculated by

$$\tau_{n,p} = \tau_n(\boldsymbol{\theta}_p) = 2\left\|\boldsymbol{x}_n - \boldsymbol{\theta}_p\right\| / c \tag{5}$$

where c is the speed of light, the additive noise $\tilde{w}_n(t)$ is usually modeled as a circularly symmetric, zero-mean, complex Gaussian white noise [58], i.e.,

$$\begin{cases} \mathbb{E}\left[\tilde{w}_n(t)\right] = 0 \\ \mathbb{E}\left[\tilde{w}_n(t) \tilde{w}_n^*(t')\right] = \sigma_{\tilde{w}}^2 \delta\left(t - t'\right) \end{cases} \tag{6}$$

where $0 < t' \leq T_{\text{pri}}$ and $\sigma_{\tilde{w}}^2$ is the noise intensity. It is assumed no targets are falling into the same delay resolution bin at each local station, i.e.,

$$\min_{\substack{(p_1,p_2)\in\{1,\ldots,P\}^2 \\ p_1 \neq p_2}} \min_{n\in\{1,\ldots,N\}} \left|\tau_n(\boldsymbol{\theta}_{p_1}) - \tau_n(\boldsymbol{\theta}_{p_2})\right| > \frac{1}{B}, \tag{7}$$

and this assumption is called *fully-separable* in this work.

Then, we employ the n-th transmitted waveform $x_n(t)$ to make matched filtering, and the continuous-time received signal at the n-th station can be output as

$$r_n(t) = \sum_{p=1}^{P} \alpha_{n,p} s_n\left(t - \tau_{n,p}\right) + w_n(t) \tag{8}$$

[2]This paper focuses on the JDL for distributed radars under communication constraints, considering a two-dimensional Cartesian coordinate system with monopulse signal model. The three-dimensional and multi-pulse (consider Doppler shifts) cases are extensible but will not be studied in this work.

[3]In order to ensure that the target's echo signal can be accurately aligned between different radar stations in distributed radar systems, the time synchronization error is assumed to be smaller than $1/(2B)$ (within a range resolution bin) [55], where B is the signal bandwidth. For example, for systems with a range resolution within a few meters, the time synchronization accuracy should be within 10 nanoseconds. For systems with higher resolution requirements, the time synchronization accuracy may be required to be less than 1 nanosecond.

[4]Attaining perfectly orthogonal waveforms may not be feasible solely through waveform design techniques in practice. However, our goal is to derive closed-form mathematical results within the JDL framework for multiple targets. While we anticipate potential localization performance degradation due to significant sidelobes, this aspect will not be examined in this study.

where $\alpha_{n,p} = \tilde{\alpha}_{n,p} e^{-\jmath 2\pi f_c \tau_{n,p}}$; $s_n(t)$ represents the matched filtering output function of $\tilde{s}_n(t)$ by employing $x_n(t)$, it exhibits a narrow-pulse characteristic in the time domain, and the auto-terms $s_n(t-\tau)$ and $s_n(t-\tau')$ are orthogonal, i.e.,

$$\int_{T_{\text{pri}}} s_n(t-\tau) s_n^*(t-\tau')\, dt \approx 0, \tau \neq \tau'. \tag{9}$$

The noise term $w_n(t)$ after matched-filtering is still the independent zero-mean white Gaussian property [31, eq. (10)] because of the assumption of thumbtack auto-correlation function, its intensity is denoted as σ_w^2.

C. Discrete-time Received Signal

Finally, the continuous-time received signal $r_n(t)$ in (8) within a PRI duration will be sampled by a sampling interval T_s. Then the overall baseband processing is completed, we can obtain $M = \lceil T/T_s \rceil$ samples of delay-dimensional observations in one frame T_{frame}, i.e.,

$$\mathbf{r}_n = \sum_{p=1}^{P} \alpha_{n,p} \mathbf{s}_n(\boldsymbol{\theta}_p) + \mathbf{w}_n. \tag{10}$$

where

$$\mathbf{r}_n = [r_n(T_s), \ldots, r_n(MT_s)]^\top \in \mathbb{C}^M, \tag{11}$$

$$\begin{aligned} \mathbf{s}_n(\boldsymbol{\theta}_p) &= \mathbf{s}_{n,p} = \mathbf{s}_n(\tau_{n,p}) \\ &= [s_n(T_s - \tau_{n,p}), \ldots, s_n(MT_s - \tau_{n,p})]^\top \in \mathbb{C}^M, \end{aligned} \tag{12}$$

$$\mathbf{w}_n = [w_n(T_s), \ldots, w_n(MT_s)]^\top \in \mathbb{C}^M, \tag{13}$$

and $\mathbf{w}_n[m] \sim \mathcal{CN}(0, \sigma_w^2)$, $m = 1, \ldots, M$. In this work, the unknown target number is assumed as $P \ll M$, the noise variance σ_w^2 is assumed known, and $\mathbf{w}_n$ is a complex circularly-symmetric white Gaussian vector with covariance $\mathbf{R}_n = \sigma_w^2 \mathbf{I}_M$, i.e., $\mathbf{w}_n \sim \mathcal{CN}(\mathbf{0}, \mathbf{R}_n)$. This model is well-suited for homogeneous environments, such as air-search mode. In more practice, the unknown noise covariance matrix can be estimated by using secondary data [23], [59].

In the following sections, we will introduce the procedures of JDL with different cases under unlimited or limited communication rates.

III. Joint Detection and Localization with Unlimited Communication Rates

In this section, we aim to jointly detect and localize multiple targets without any communication constraints between each local radar and the FC. Firstly, we elaborate a GLRT detector for the distributed radars to detect and localize multiple targets simultaneously, but it is computationally intractable. Then, we employ a successive interference cancellation (SIC) solution to solve the high-computational problem. Finally, we analyze the computational of the high-dimensional GLRT detector and the low-dimensional solution, and then the calculation of the actual occupied communication rates is also given.

A. Multi-Target GLRT Detector

It can be seen from (10) that the delay-dimensional observations $\mathbf{r}_n$ is the noisy superposition of the signals originated from P targets, where $P = 1, \ldots, P_{\max}$ and $P_{\max} \geq 1$ is the assumed upper bound of the unknown prospective target number. Thus we can consider a composite multiple hypotheses testing problem, namely,

$$\begin{cases} \mathcal{H}_0 : \mathbf{r}_n = \mathbf{w}_n, \ \forall\, n \\ \mathcal{H}_1 : \mathbf{r}_n = \alpha_{n,1} \mathbf{s}_n(\boldsymbol{\theta}_1) + \mathbf{w}_n, \ \forall\, n \\ \qquad \vdots \\ \mathcal{H}_{P_{\max}} : \mathbf{r}_n = \sum_{p=1}^{P_{\max}} \alpha_{n,p} \mathbf{s}_n(\boldsymbol{\theta}_p) + \mathbf{w}_n, \ \forall\, n \end{cases} \tag{14}$$

where $\mathcal{H}_0$ is the target-absent hypothesis and $\mathcal{H}_P$ is the hypothesis that P targets are present (for $P = 1, \ldots, P_{\max}$). As customary, we assume that the prospective targets are located on finite $Q_{\mathcal{G}}$ grids [26], [60] in the inspected location region $\mathcal{G}$, and the grids are uniformly-spaced and have an inter-element spacing $\Delta_g \leq c/2B$ in the inspected region, i.e., $\boldsymbol{\theta}_p \in \mathcal{G}$, $\forall p$. Here, we denote $\boldsymbol{\alpha}_{n,1:P} = [\alpha_{n,1}, \ldots, \alpha_{n,P}]^\top$ as the vector of unknown complex reflection coefficients. Additionally, we denote $\boldsymbol{\theta}_{1:P} = \text{cat}\{\boldsymbol{\theta}_1, \ldots, \boldsymbol{\theta}_P\} \in \mathcal{G}_{1:P}$ as the vector of unknown locations of the actual existing targets, where

$$\begin{aligned} \mathcal{G}_{1:P} = \Big\{ &\text{cat}\{\boldsymbol{\theta}_1, \ldots, \boldsymbol{\theta}_P\} \in \mathcal{G}^P : \\ &\min_{\substack{(p_1,p_2)\in\{1,\ldots,P\}^2 \\ p_1 \neq p_2}} \min_{n\in\{1,\ldots,N\}} \left| \tau_n(\boldsymbol{\theta}_{p_1}) - \tau_n(\boldsymbol{\theta}_{p_2}) \right| > 1/B \Big\} \end{aligned} \tag{15}$$

is the set specifying all possible positions of the targets.

Here we analyze the distribution of the signal vector $\mathbf{r}_n$ under different hypotheses, i.e.,

$$\begin{cases} \mathcal{H}_0 : \mathbf{r}_n \sim \mathcal{CN}(\mathbf{0}, \mathbf{R}_n) \\ \mathcal{H}_P : \mathbf{r}_n \sim \mathcal{CN}\left(\sum_{p=1}^{P} \alpha_{n,p} \mathbf{s}_n(\boldsymbol{\theta}_p), \mathbf{R}_n \right), \end{cases} \tag{16}$$

where $P = 1, \ldots, P_{\max}$.

The probability density function (PDF) of $\mathbf{r}_n$ can be written as [12], [23], [35], [37], [59]

$$\mathrm{p}(\mathbf{r}_n \mid \mathcal{H}_0) = \frac{1}{\pi^M \det(\mathbf{R}_n)} \exp\left\{ -(\mathbf{r}_n)^H \mathbf{R}_n^{-1} \mathbf{r}_n \right\} \tag{17}$$

and

$$\begin{aligned} &\mathrm{p}(\mathbf{r}_n \mid \boldsymbol{\theta}_{1:P}, \boldsymbol{\alpha}_{n,1:P}, \mathcal{H}_P) \\ &\quad = \frac{1}{\pi^M \det(\mathbf{R}_n)} \exp\Big\{ -(\mathbf{r}_n - \mathbf{S}_{n,1:P} \boldsymbol{\alpha}_{n,1:P})^H \\ &\qquad\qquad \times \mathbf{R}_n^{-1} (\mathbf{r}_n - \mathbf{S}_{n,1:P} \boldsymbol{\alpha}_{n,1:P}) \Big\} \end{aligned} \tag{18}$$

under the hypotheses $\mathcal{H}_0$ and $\mathcal{H}_P$, $P = 1, \ldots, P_{\max}$, respectively, where $\mathbf{S}_{n,1:P} = [\mathbf{s}_n(\boldsymbol{\theta}_1), \ldots, \mathbf{s}_n(\boldsymbol{\theta}_P)] \in \mathbb{C}^{M \times P}$ and $\mathbf{S}_{n,1:P} \boldsymbol{\alpha}_{n,1:P} = \sum_{p=1}^{P} \alpha_{n,p} \mathbf{s}_n(\boldsymbol{\theta}_p)$.

Remark 1. The derivations of (17) and (18) are valid for the given complex circularly-symmetric white Gaussian noise assumption, which imposes the uncorrelated property of the real and imaginary components and consequently yields a diagonal covariance matrix $\mathbf{R}_n$. The noise assumption, along with the same PDF structures, has also been widely adopted in prior works, including [12], [23], [35], [37], [59].

To get the estimation of $\boldsymbol{\theta}_{1:P}$, the LLR function [61] is derived as:

$$\begin{aligned}\ln\ \mathcal{L}\left(\mathbf{r}_n \mid \boldsymbol{\theta}_{1:P}, \boldsymbol{\alpha}_{n,1:P}\right) \propto \ln\ \frac{\mathrm{p}(\mathbf{r}_n \mid \boldsymbol{\theta}_{1:P}, \boldsymbol{\alpha}_{n,1:P}, H_P)}{\mathrm{p}(\mathbf{r}_n \mid H_0)} \\ = \mathbf{r}_n^H \mathbf{R}_n^{-1} \mathbf{S}_{n,1:P} \boldsymbol{\alpha}_{n,1:P} + \boldsymbol{\alpha}_{n,1:P}^H \mathbf{S}_{n,1:P}^H \mathbf{R}_n^{-1} \mathbf{r}_n \\ - \boldsymbol{\alpha}_{n,1:P}^H \mathbf{S}_{n,1:P}^H \mathbf{R}_n^{-1} \mathbf{S}_{n,1:P} \boldsymbol{\alpha}_{n,1:P}.\end{aligned} \tag{19}$$

We denote the maximum likelihood (ML) estimate of $\boldsymbol{\alpha}_{n,1:P}$ as $\hat{\boldsymbol{\alpha}}_{n,1:P}$, which can be calculated by

$$\frac{\partial}{\partial \boldsymbol{\alpha}_{n,1:P}} \ln \mathcal{L}\left(\mathbf{r}_n \mid \boldsymbol{\theta}_{1:P}, \boldsymbol{\alpha}_{n,1:P}\right)\Big|_{\boldsymbol{\alpha}_{n,1:P}=\hat{\boldsymbol{\alpha}}_{n,1:P}} = \mathbf{0}. \tag{20}$$

Then, $\hat{\boldsymbol{\alpha}}_{n,1:P}$ can be obtained in closed-form [35], i.e.,

$$\hat{\boldsymbol{\alpha}}_{n,1:P} = \left(\mathbf{S}_{n,1:P}^H \mathbf{R}_n^{-1} \mathbf{S}_{n,1:P}\right)^+ \mathbf{S}_{n,1:P}^H \mathbf{R}_n^{-1} \mathbf{r}_n. \tag{21}$$

After plugging (21) into (19), the LLR function can be rewritten as

$$\begin{aligned}\ln \mathcal{L}\left(\mathbf{r}_n \mid \boldsymbol{\theta}_{1:P}, \hat{\boldsymbol{\alpha}}_{n,1:P}\right) =& \mathbf{r}_n^H \mathbf{R}_n^{-1} \mathbf{S}_{n,1:P} \left(\mathbf{S}_{n,1:P}^H \mathbf{R}_n^{-1}\right. \\ & \left. \times \mathbf{S}_{n,1:P}\right)^+ \mathbf{S}_{n,1:P}^H \mathbf{R}_n^{-1} \mathbf{r}_n.\end{aligned} \tag{22}$$

Given the uncertainty of the target number P, we employ a generalized information criterion (GIC) [62], [63] to estimate both the number and locations of targets. The estimates of the number and locations of targets, denoted by $\hat{P}$ and $\hat{\boldsymbol{\theta}}_{1:\hat{P}} = \mathrm{cat}\{\hat{\boldsymbol{\theta}}_1, \ldots, \hat{\boldsymbol{\theta}}_{\hat{P}}\}$, respectively, can be derived as follows:

$$\hat{P} = \underset{P \in \{0,\ldots,P_{\max}\}}{\arg\max}\ \mathrm{GIC}(P) \tag{23}$$

where

$$\mathrm{GIC}(P) = \begin{cases} \sum\limits_{n=1}^{N} \ln \mathrm{p}(\mathbf{r}_n \mid \mathcal{H}_0), & P = 0 \\ \max\limits_{\boldsymbol{\theta}_{1:P} \in \mathcal{G}_{1:P}} \sum\limits_{n=1}^{N} \ln \mathcal{L}\left(\mathbf{r}_n \mid \boldsymbol{\theta}_{1:P}, \hat{\boldsymbol{\alpha}}_{n,1:P}\right) & \\ \qquad\qquad - NP\eta, & P \geq 1, \end{cases} \tag{24}$$

and

$$\hat{\boldsymbol{\theta}}_{1:\hat{P}} = \underset{\boldsymbol{\theta}_{1:\hat{P}} \in \mathcal{G}_{1:\hat{P}}}{\arg\max} \sum_{n=1}^{N} \ln \mathcal{L}\left(\mathbf{r}_n \mid \boldsymbol{\theta}_{1:\hat{P}}, \hat{\boldsymbol{\alpha}}_{n,1:\hat{P}}\right) - N\hat{P}\eta, \tag{25}$$

if $\hat{P} \geq 1$. In (24), η is the penalty factor set to satisfy a given probability of false alarm $\mathrm{P_{fa}} = \Pr(\text{reject } \mathcal{H}_0 | \mathcal{H}_0)$.

Hence, from (23), (24), and (25), we can see that a high-dimensional search for estimating the unknown target number P and locations $\boldsymbol{\theta}_{1:P} \in \mathcal{G}_{1:P}$ is implemented. Once $\hat{P}$ is declared by (23): if $\hat{P} \geq 1$, the corresponding locations $\hat{\boldsymbol{\theta}}_{1:\hat{P}}$ will be output; otherwise, no targets are declared.

Remark 2. The multi-target GLRT detector can theoretically realize the simultaneous detection and localization of targets and output their estimated number and locations at once. However, it is computationally prohibitive in practical implementation as it is devoted to solving the joint maximization task of $(Q_{\mathcal{G}})^P$ $(P = 1, \ldots, P_{\max})$ grids, i.e., calculating $\max_{\boldsymbol{\theta}_{1:P} \in \mathcal{G}_{1:P}}$ in (24). In Section III-B, a low-dimensional solution will be introduced to simplify this high-dimensional search problem. Besides, Section III-C1 provides the computational comparison of the high- and low-dimensional ways.

Remark 3. In the high-dimensional case, only the delay-dimensional observations $\mathbf{r}_n$ are suitable for transmission from each station to the FC for data fusion. Since an extensive search over P and $\boldsymbol{\theta}_{1:P} \in \mathcal{G}_{1:P}$ need to be performed at the FC, different possibilities of P and $\boldsymbol{\theta}_{1:P}$ will result in different sizes of $\mathbf{S}_{n,1:P}$ and corresponding LLR values of (22). It is impractical for the high-dimensional case to generate the LLR data with different possibilities at each local station. Instead, the low-dimensional solution in the next subsection involves generating standardized and discrete LLR data and transmitting them to the FC.

B. Low-Dimensional Solution

In this subsection, a low-dimensional solution will be introduced. The joint maximization task of $(Q_{\mathcal{G}})^P$ grids in the high-dimensional detector will be partitioned into P separate optimization problems of $Q_{\mathcal{G}}$ grids. Given the *fully-separable* assumption in (7) and the orthogonal property[5] in (9), the terms $\mathbf{s}_n(\boldsymbol{\theta}_{p_1})$ and $\mathbf{s}_n(\boldsymbol{\theta}_{p_2})$ satisfy the following condition [35],

$$\mathbf{s}_n^H(\boldsymbol{\theta}_{p_1}) \mathbf{R}_n^{-1} \mathbf{s}_n(\boldsymbol{\theta}_{p_2}) \approx 0\,. \tag{26}$$

Then, the matrix $\mathbf{S}_{n,1:P}^H \mathbf{R}_n^{-1} \mathbf{S}_{n,1:P}$ can be obtained as

$$\begin{aligned}&\mathbf{S}_{n,1:P}^H \mathbf{R}_n^{-1} \mathbf{S}_{n,1:P} \\ &= \begin{bmatrix} \mathbf{s}_{n,1}^H \mathbf{R}_n^{-1} \mathbf{s}_{n,1} & 0 & \cdots & 0 \\ 0 & \mathbf{s}_{n,2}^H \mathbf{R}_n^{-1} \mathbf{s}_{n,2} & \cdots & 0 \\ \vdots & \vdots & \ddots & \vdots \\ 0 & 0 & \cdots & \mathbf{s}_{n,P}^H \mathbf{R}_n^{-1} \mathbf{s}_{n,P} \end{bmatrix}.\end{aligned} \tag{27}$$

After plugging (27) into (21), we obtain

$$\hat{\alpha}_{n,p} = \frac{\mathbf{s}_{n,p}^H \mathbf{R}_n^{-1} \mathbf{r}_n}{\mathbf{s}_{n,p}^H \mathbf{R}_n^{-1} \mathbf{s}_{n,p}}. \tag{28}$$

Substituting (28) back into (19), we have

$$\begin{aligned}\ln \mathcal{L}\left(\mathbf{r}_n \mid \boldsymbol{\theta}_{1:P}, \hat{\boldsymbol{\alpha}}_{n,1:P}\right) &= \mathbf{r}_n^H \mathbf{R}_n^{-1} \sum_{p=1}^{P} \hat{\alpha}_{n,p} \mathbf{s}_{n,p} \\ &= \sum_{p=1}^{P} \frac{\left|\mathbf{s}_{n,p}^H \mathbf{R}_n^{-1} \mathbf{r}_n\right|^2}{\mathbf{s}_{n,p}^H \mathbf{R}_n^{-1} \mathbf{s}_{n,p}}.\end{aligned} \tag{29}$$

Same as (25), we can have

$$\begin{aligned}\hat{\boldsymbol{\theta}}_{1:P} &= \mathrm{cat}\{\hat{\boldsymbol{\theta}}_1, \ldots, \hat{\boldsymbol{\theta}}_P\} \\ &= \underset{\boldsymbol{\theta}_{1:P} \in \mathcal{G}_{1:P}}{\arg\max} \sum_{n=1}^{N} \sum_{p=1}^{P} \frac{\left|\mathbf{s}_{n,p}^H \mathbf{R}_n^{-1} \mathbf{r}_n\right|^2}{\mathbf{s}_{n,p}^H \mathbf{R}_n^{-1} \mathbf{s}_{n,p}} - NP\eta \\ &= \underset{\boldsymbol{\theta}_{1:P} \in \mathcal{G}_{1:P}}{\arg\max} \sum_{p=1}^{P} \sum_{n=1}^{N} \ell_n\left(\boldsymbol{\theta}_p\right) - NP\eta \\ &= \underset{\boldsymbol{\theta}_{1:P} \in \mathcal{G}_{1:P}}{\arg\max} \sum_{p=1}^{P} \mathcal{D}\left(\boldsymbol{\theta}_p\right) - NP\eta\end{aligned} \tag{30}$$

[5]This orthogonal assumption neglects the effect of sidelobes in the auto-correlation functions of practical waveforms, which had been investigated in our previous work [36].

where

$$\mathcal{D}\left(\boldsymbol{\theta}_p\right)=\sum_{n=1}^{N}\ell_n\left(\boldsymbol{\theta}_p\right), \tag{31}$$

and

$$\ell_n\left(\boldsymbol{\theta}_p\right)=\frac{\left|\mathbf{s}_{n,p}^H\mathbf{R}_n^{-1}\mathbf{r}_n\right|^2}{\mathbf{s}_{n,p}^H\mathbf{R}_n^{-1}\mathbf{s}_{n,p}} \tag{32}$$

are the objective LLR functions of the p-th target location $\boldsymbol{\theta}_p$ regarding all stations and the n-th station. It should be noted that the targets $\boldsymbol{\theta}_{1:P}\in\mathcal{G}_{1:P}$ follow the relationship presented in (7) and (15).

In practical implementation, given the unknown number, amplitudes, and locations of multiple targets, we should extract them from the objective LLR function regarding N stations and all grid points within the inspected location region $\mathcal{G}$, i.e.,

$$\mathcal{D}\left(\boldsymbol{\theta}\right)=\sum_{n=1}^{N}\ell_n\left(\boldsymbol{\theta}\right)=\sum_{n=1}^{N}\frac{\left|\mathbf{s}_n^H(\boldsymbol{\theta})\mathbf{R}_n^{-1}\mathbf{r}_n\right|^2}{\mathbf{s}_n^H(\boldsymbol{\theta})\mathbf{R}_n^{-1}\mathbf{s}_n(\boldsymbol{\theta})},\boldsymbol{\theta}\in\mathcal{G}. \tag{33}$$

The extraction implementation is given in (37). Before the implementation, the LLR function $\ell_n(\boldsymbol{\theta})$ can be calculated in a standardized and discrete manner at the n-th local station without considering the value changing of $\boldsymbol{\theta}$. More precisely, the resulting original delay-dimensional LLR data vector $\mathbf{L}_n$, is discretely calculated by relating to different delay bins and will be transmitted from the local station to the FC, i.e.,

$$\mathbf{L}_n\triangleq\left[L_n[1],L_n[2],\ldots,L_n[m],\ldots,L_n[M]\right]^\top \tag{34}$$

where

$$\begin{aligned}L_n[m]&=\ell_n\left(\boldsymbol{\theta}\mid\tau_n^m\right)\\&=\frac{\left|\mathbf{s}_n^H(\tau_n^m)\mathbf{R}_n^{-1}\mathbf{r}_n\right|^2}{\mathbf{s}_n^H(\tau_n^m)\mathbf{R}_n^{-1}\mathbf{s}_n(\tau_n^m)}\end{aligned} \tag{35}$$

for $n=1,\ldots,N$, $m=1,\ldots,M$, and $\tau_n^m=mT_s$. Therefore, in practice, local stations can undertake a portion of calculations and the FC will receive the LLR data $\mathbf{L}_n\in\mathbb{C}^M,n=1,\ldots,N$ from different stations to make *data association*. Then, (33) can be rewritten as

$$\mathcal{D}\left(\boldsymbol{\theta}\right)=\sum_{n=1}^{N}L_n[\lceil\tau_n(\boldsymbol{\theta})/T_s\rceil],\boldsymbol{\theta}\in\mathcal{G}. \tag{36}$$

Remark 4. In (36), the FC receives different LLR data vectors $\mathbf{L}_n\in\mathbb{C}^M,n=1,\ldots,N$ and proceeds to perform LLR *data association*. Given that the FC possesses knowledge about the locations of local stations, for a specific grid $\boldsymbol{\theta}\in\mathcal{G}$ at the FC, we can calculate $\lceil\tau_n(\boldsymbol{\theta})/T_s\rceil$ to determine its corresponding values in different $\mathbf{L}_n$. Then we extract and add them together, thus the *data association* at the FC has been implemented.

At the FC, a location data plane can be generated by traversing $\mathcal{D}\left(\boldsymbol{\theta}\right)$ in (36) with different $\boldsymbol{\theta}\in\mathcal{G}$. The challenge we face now is how to extract multiple targets from this data plane. Given the *fully-separable* assumption that no targets fall into the same resolution bin at any station, an efficient method to avoid simultaneous and extensive searching is to identify the maximum LLR value at each iteration upon reducing the impact of LLR data from other targets. Each iteration extracts one target and estimates its location $\hat{\boldsymbol{\theta}}_p$, $p=1,\ldots,\hat{P}$, where $\hat{P}$ will be declared finally, thus realizing detection and localization of every target. The detector can be computed as

$$\begin{aligned}&\hat{\boldsymbol{\theta}}_{1:\hat{P}}=\text{cat}\{\hat{\boldsymbol{\theta}}_1,\ldots,\hat{\boldsymbol{\theta}}_{\hat{P}}\}\\&\text{with}\quad\hat{\boldsymbol{\theta}}_p=\underset{\boldsymbol{\theta}\in\mathcal{G}}{\arg\max}\ \mathcal{D}_p\left(\boldsymbol{\theta}\right)\\&\text{s.t.}\quad\underset{\boldsymbol{\theta}\in\mathcal{G}}{\max}\ \mathcal{D}_p\left(\boldsymbol{\theta}\right)\geq\psi,\ p\leq P_{\max}\end{aligned} \tag{37}$$

where ψ is the detection threshold set to obtain a desired constant false alarm probability, namely,

$$\mathrm{P_{fa}}=\Pr(\underset{\boldsymbol{\theta}\in\mathcal{G}}{\max}\ \mathcal{D}(\boldsymbol{\theta})>\psi\ \big|\ \mathcal{H}_0), \tag{38}$$

and $\mathcal{D}_p\left(\boldsymbol{\theta}\right)$ denotes the p-th updated LLR function.

Here the iterative extraction and estimation of targets can be elaborated by multiple steps:

1) **Step 1**: At the p-th iteration, traverse $\mathcal{D}_p\left(\boldsymbol{\theta}\right)$ ($p=1,\ldots,P_{\max}$ and $\mathcal{D}_1\left(\boldsymbol{\theta}\right)=\mathcal{D}\left(\boldsymbol{\theta}\right)$) with different $\boldsymbol{\theta}\in\mathcal{G}$, thus generating a location data plane including $Q_\mathcal{G}$ grids;
2) **Step 2**: Find the maximum value of the location data plane. If it exceeds the preset threshold ψ, the p-th target is declared and the corresponding location $\boldsymbol{\theta}_p$ will be extracted as its estimation $\hat{\boldsymbol{\theta}}_p$;
3) **Step 3**: Remove the data of the identified target within a delay resolution bin and generate a new LLR function to extract the $(p+1)$-th target, i.e.,

$$\begin{aligned}\mathcal{D}_{p+1}(\boldsymbol{\theta})&=\mathcal{D}_p(\boldsymbol{\theta})-\sum_{n=1}^{N}\mathcal{X}_{n,p}\left(\boldsymbol{\theta},\hat{\boldsymbol{\theta}}_p\right)\\&=\mathcal{D}(\boldsymbol{\theta})-\sum_{n=1}^{N}\sum_{i=1}^{p}\mathcal{X}_{n,i}\left(\boldsymbol{\theta},\hat{\boldsymbol{\theta}}_i\right),\end{aligned} \tag{39}$$

where

$$\mathcal{X}_{n,p}\left(\boldsymbol{\theta};\hat{\boldsymbol{\theta}}_p\right)=\begin{cases}L_n[\lceil\tau_n(\boldsymbol{\theta})/T_s\rceil],\boldsymbol{\theta}\in\mathbb{B}_n\left(\boldsymbol{\theta};\hat{\boldsymbol{\theta}}_p\right)\\0,\qquad\qquad\text{others}\end{cases} \tag{40}$$

and

$$\mathbb{B}_n\left(\boldsymbol{\theta};\hat{\boldsymbol{\theta}}_p\right)=\left\{\boldsymbol{\theta}\big|\ \mid\tau_n(\boldsymbol{\theta})-\tau_n(\hat{\boldsymbol{\theta}}_p)\mid\leq1/B,\boldsymbol{\theta}\in\mathcal{G}\right\}; \tag{41}$$

4) **Step 4**: Repeat the previous steps until the maximum value does not exceed the threshold or p exceeds $P_{\max}$. Finally, output the estimated number of targets $\hat{P}=p-1$ and all estimated locations $\hat{\boldsymbol{\theta}}_{1:\hat{P}}$.

As a result, the JDL-UCR employing the low-dimensional solution has been elaborated. The joint maximization task of $(Q_\mathcal{G})^P$ grids in the high-dimensional detector has been partitioned into P separate optimization problems of $Q_\mathcal{G}$ grids. For the reader's sake, the overall structure is shown in Fig. 2(a).

C. Discussion

1) Computational Analysis: We assume that the matrix $\mathbf{R}_n^{-1}$ and the whitened measurement $\mathbf{R}_n^{-1}\mathbf{r}_n$ are precomputed and stored in dedicated memory. First, we analyze the computational expenses of the high-dimensional multi-target GLRT detector. Assuming there are P targets, the calculation

of the LLR equation in (22) for each station incurs a cost of $\mathcal{O}\big(PM^2+P^2M+P^3\big)$ floating point operations (flops). Consequently, the total cost for computing the ML detection and estimation in (25) for N stations and the inspected $(Q_{\mathcal{G}})^P$ possibilities is at least $\mathcal{O}\big(N(PM^2+P^2M+P^3)(Q_{\mathcal{G}})^P\big)$ flops. Since P is unknown and needs to be estimated, the computational expenses will increase exponentially as P increases.

Instead, for the low-dimensional solution, the primary factor computational expense is driven by the calculation of the objective LLR function $\mathcal{D}(\boldsymbol{\theta})$ in (36). The computational load of (35) is bounded by $\mathcal{O}\big(M^2\big)$ flops. Given that $\mathbf{L}_n$ in (34) contains M points, the total computational load for computing the LLR data matrix at all local stations is $\mathcal{O}\big(NM^3\big)$. At the FC, the cost for computing $\mathcal{D}(\boldsymbol{\theta})$ regarding N stations and the inspected $Q_{\mathcal{G}}$ grids is $\mathcal{O}\big(NQ_{\mathcal{G}}\big)$ flops. Additionally, updating the objective LLR function at each iteration incurs $\mathcal{O}\big(NQ_{\mathcal{G}}\big)$ flops. Finally, considering there are P times of potential loops, the total cost for computing the low-dimensional solution is at least $\mathcal{O}\big(NM^3+NPQ_{\mathcal{G}}\big)$ flops.

Comparing the two computational analysis results, i.e., $\mathcal{O}\big(N(PM^2+P^2M+P^3)(Q_{\mathcal{G}})^P\big)$ and $\mathcal{O}\big(NM^3+NPQ_{\mathcal{G}}\big)$, it is obvious that the low-dimensional solution requires much less computation and will be better for the practical implementation of JDL of multiple targets.

2) Communication Rates Analysis: Here we analyze the communication rates between each radar and the FC when employing the JDL-UCR with low-dimensional solution. We assume the LLR data in (34) will be re-quantized by $\gamma = \gamma_1+\gamma_2$ bits per point before transmission, where γ_1 and γ_2 quantize the index of each delay bin and the amplitude of corresponding sample, respectively. It is known from the previous system and signal model texts that the duration and total number of samples per frame are T_{frame} and M, respectively. To ensure the real-time nature of information processing, as illustrated in Fig. 3, it is assumed that once the received signals of each PRI are obtained, the data processing at each radar, LLR data transmission, and global decision at the FC are completed within the time $T_{\text{frame}} = T_{\text{local}}+T_{\text{tran}}+T_{\text{FC}}$, where T_{local} is the time for local signal processing, T_{tran} for data transmission, and T_{FC} for global decision. Therefore, the actual communication rates per second between the n-th local radar and the FC are

$$W_n^{\text{UCR}} = \frac{M\gamma}{T_{\text{tran}}} \text{ bps}. \tag{42}$$

IV. Joint Detection and Localization with an Efficient Censoring Method under Communication Constraints

In this section, we propose a JDL-ECM algorithm to realize high detection performance and localization accuracy under the environment of communication constraints between each local radar and the FC. Fig. 3 presents the timeline of the signal processing and data transmission for one frame. It should be noted that, when the communication constraints appear between local radars and the FC, it is difficult to transmit complete LLR data within T_{tran}. Therefore, it is necessary to compress the data to accommodate the constraints. Then we devote to devising an efficient censoring method to compress the LLR data, and the decision information of the previous frame is leveraged to make the retained small parts of LLR data more informative. Consequently, this approach realizes the advantages of low-rate communication and high-performance detection/localization of multiple targets.

For the reader's convenience, Figs. 2(a) and (b) report

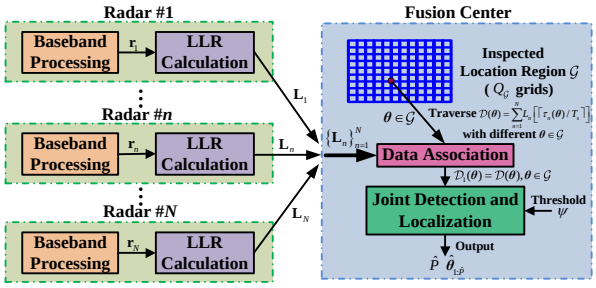

(a) The structure of the JDL-UCR (no communication constraints).

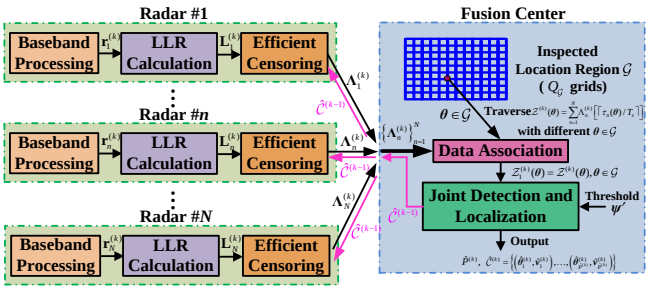

(b) The structure of the JDL-ECM (under communication constraints).

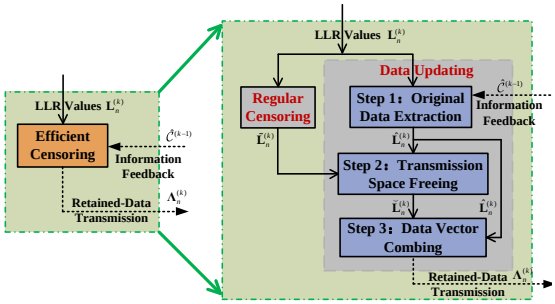

(c) Detailed illustration of the efficient censoring method.

Figure 2. The illustrations of the JDL-UCR algorithm, the JDL-ECM algorithm, and the detailed content of the efficient censoring method. This method contains two main parts: regular censoring and data updating. The data updating part contains three steps: original data extraction, transmission space freeing, and data vectors combing.

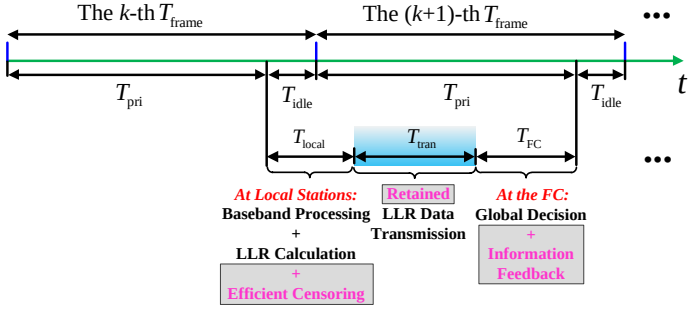

Figure 3. The timeline of the signal processing and data transmission for one frame when the JDL-ECM/JDL-UCR algorithms are employed (Omit the contents in the rectangles when employing the JDL-UCR algorithm).

the structures of the JDL-UCR and JDL-ECM algorithms. Unlike the JDL-UCR, which transmits the complete original LLR data, the JDL-ECM uses efficient censoring and information feedback to filter most LLR values and transmit only the retained informative data to the FC, in line with specific communication rates. The efficient censoring method in Fig. 2(c) has two main steps: first, applying a CFAR-based censoring rule to preprocess LLR vectors and keep only low-rate informative data; second, utilizing previously estimated target locations and velocities fed back by the FC to enhance the effectiveness of the retained data in the current frame.

To establish a premise, we assume $\Upsilon_n \ll W_n^{\text{UCR}}$ is the constant limited communication rate between the n-th local radar and the FC. To make full use of the limited rate, we define a data retaining percentage to compress the complete data required by the JDL-UCR, which is calculated by

$$\mathrm{P}_{\text{re},n} = \Upsilon_n / W_n^{\text{UCR}} \times 100\%. \tag{43}$$

Then, the upper limit on the number of samples (their values are also quantized by γ bits), which could be retained per frame and transmitted to the FC during the LLR data transmission time T_{tran}, can be outputted as

$$V_{\text{re},n} = \lfloor M \mathrm{P}_{\text{re},n} \rfloor. \tag{44}$$

Besides, it is assumed that γ_3 bits are required to quantize the feedback information per frame, e.g., the estimated locations and velocities in the feedback information set $\hat{\boldsymbol{\mathcal{C}}} = \{(\hat{\boldsymbol{\theta}}_1, \hat{\boldsymbol{v}}_1), \ldots, (\hat{\boldsymbol{\theta}}_{\hat{P}}, \hat{\boldsymbol{v}}_{\hat{P}})\}$, which is generated by the FC at each frame. The small-volume feedback information at the FC is assumed to be fully fed back to the radars within sufficient time allocated in T_{FC} and under the communication constraints[6].

A. Regular Censoring

Now we face the censoring problem of the original LLR data $\mathbf{L}_n^{(k)}$ at the k-th ($k = 1, \ldots, K_{\max}$) frame, where $K_{\max}$ is the assumed total frames number used for performance analyses, we formulate the following regular censoring rule:

$$\tilde{L}_n^{(k)}[m] = \begin{cases} L_n^{(k)}[m], & \text{if } \left| L_n^{(k)}[m] \right| \geq \rho_{n,m}^{(k)} \\ \text{null}, & \text{else} \end{cases}, \forall n, m. \tag{45}$$

where null is defined as 'empty', i.e., no quantization and transmission, $\tilde{L}_n^{(k)}[m] \in \tilde{\mathbf{L}}_n^{(k)}$,

$$\tilde{\mathbf{L}}_n^{(k)} \triangleq \left[\tilde{L}_n^{(k)}[1], \ldots, \tilde{L}_n^{(k)}[m], \ldots, \tilde{L}_n^{(k)}[M] \right]^\top \tag{46}$$

is the remained LLR data after censoring, and $\rho_{n,m}^{(k)}$ is the censoring threshold for the m-th element of LLR data at the k-th frame and the n-th local radar. Briefly, this rule is to establish adaptive censoring thresholds and filter out the data which can't exceed. Therefore, the relationship between $\rho_{n,m}^{(k)}$ and the data retaining percentage $\mathrm{P}_{\text{re},n}$ in (43) is represented as

$$\mathrm{P}_{\text{re},n} = \Pr(\left| L_n^{(k)}[m] \right| \geq \rho_{n,m}^{(k)}, \forall k, m). \tag{47}$$

Remark 5. Since $\mathrm{P}_{\text{re},n}$ is already known based on the given limited communication rate Υ_n, i.e., using (44) and (43), the problem we face now is how to calculate the adaptive censoring thresholds $\rho_{n,m}^{(k)}, \forall n, m$. The expected situation is that the actual proportion of the retained non-null LLR data, after being censored by $\rho_{n,m}^{(k)}, \forall n, m$, can be stable and perfectly matches the given data retaining percentage at each frame, so that the informative data can be retained as much as possible under communication constraints.

Remark 6. To achieve this expected situation, we employ the CFAR detection method to treat the given data retaining percentage $\mathrm{P}_{\text{re},n}$ as the local false alarm probability. It ensures the number of false alarms aligns with the expected retained value $V_{\text{re},n}$ (e.g., for $M = 1500$ and $\mathrm{P}_{\text{re},n} = 2\%$, $V_{\text{re},n} = \lfloor M \mathrm{P}_{\text{re},n} \rfloor = 30$). Given the assumption $P \ll M$, the detected targets minimally impact the actual retained data count. If the actual number exceeds the upper limit, **Step 2** in the next subsection will filter out smaller points to maintain the cap. Thus, the mixed false alarms and detected target points will be retained with non-null amplitudes in (46). Consequently, the problem of calculating adaptive censoring thresholds is converted into determining low detection thresholds based on a specified high local false alarm probability, addressed in the following Propositions.

Proposition 1. Given the thumbtack auto-correlation assumption of waveforms (i.e., the orthogonal property in (9)), the known noise covariance $\mathbf{R}_n = \sigma_w^2 \mathbf{I}_M$, the original LLR data $\mathbf{L}_n^{(k)}$, and the data retaining percentage $\mathrm{P}_{\text{re},n}$, the closed-form censoring thresholds will be determined as

$$\rho_{n,m}^{(k)} = -\ln \mathrm{P}_{\text{re},n}, \tag{48}$$

for $m = 1, 2, \ldots, M$ and $n = 1, \ldots, N$.

The proof of Proposition 1 is given in the Appendix A.

Proposition 2. When the waveform assumption is relaxed or a homogeneous environment with unknown noise covariance is considered in practice, deriving closed-form censoring thresholds becomes challenging. In this case, the widely used cell-averaging CFAR (CA-CFAR) detection method in [64] can be employed as an adaptive censoring rule. Given the original LLR data $\mathbf{L}_n^{(k)}$, data retaining percentage $\mathrm{P}_{\text{re},n}$, and the assumed number of one-sided adjacent reference cells D, the adaptive censoring thresholds can be determined as follows:

$$\rho_{n,m}^{(k)} = \sqrt{(\mathrm{P}_{\text{re},n}^{-\frac{1}{2D}} - 1) \sum_{d=1}^{D} (\left| L_n^{(k)}[m-d] \right|^2 + \left| L_n^{(k)}[m+d] \right|^2)}, \tag{49}$$

for $m = 1, 2, \ldots, M$ and $n = 1, \ldots, N$.

The proof of Proposition 2 is given in the Appendix B.

B. Data Updating

From the previous section, we can see the LLR data can be regularly censored by the CFAR-based censoring rule,

[6]Since feedback process only transmits γ_3 bits per frame to each radar, its transmission can be finished under communication constraints if enough time is reserved in T_{FC}. Moreover, the allocation of processing/transmission/decision times (T_{local}/T_{tran}/T_{FC}) in Fig. 3 depends on the system hardware's processing performance. It is left to the engineers responsible for implementation and is beyond the scope of this paper.

only retaining the relatively informative data. However, the informative data may not be effectively extracted especially when the system is under low-SNR environment. Once the target data of some paths are not extracted, it may have a relatively large impact on global performance. At this time, the global detection and localization results output by the FC in the past few frames may provide good hints. We can feed back the estimated locations and velocities (if any targets were detected by the FC at the past several frames) to each radar for the updating of the retained data $\tilde{\mathbf{L}}_n^{(k)}$, making the final extracted data more informative.

Before proceeding with the data updating, a point that should be considered is that the targets are moving with constant velocities. Therefore, the targets at the current frame may not be located at the bins corresponding to the previous estimates, and we should make location predictions based on the estimated locations and velocities of previous frames at each local station. To proceed, we denote the feedback set of estimated locations and velocities of the detected targets at the i-th ($i = 1, \ldots, k-1$) frame as

$$\hat{\boldsymbol{\mathcal{C}}}^{(i)} = \{(\hat{\boldsymbol{\theta}}_1^{(i)}, \hat{\boldsymbol{v}}_1^{(i)}), \ldots, (\hat{\boldsymbol{\theta}}_{\hat{P}^{(i)}}^{(i)}, \hat{\boldsymbol{v}}_{\hat{P}^{(i)}}^{(i)})\}, \tag{50}$$

and denote the prediction set, which is original from the i-th frame and predicted output for the current k-th frame, as

$$\hat{\boldsymbol{\mathcal{B}}}^{(k,i)} = \{\tilde{\boldsymbol{\theta}}_1^{(k,i)}, \ldots, \tilde{\boldsymbol{\theta}}_{\hat{P}^{(i)}}^{(k,i)}\} \tag{51}$$

where

$$\tilde{\boldsymbol{\theta}}_p^{(k,i)} = \hat{\boldsymbol{\theta}}_p^{(i)} + (k-i) T_{\text{frame}} \hat{\boldsymbol{v}}_p^{(i)} \tag{52}$$

for $p = 1, \ldots, \hat{P}^{(i)}$.

Then, utilizing a sliding window length $q \geq 1$ to represent the number of previous frames for the data updating, we denote the union of the prediction sets by

$$\boldsymbol{\Gamma}^{(k)} = \begin{cases} \varnothing, k = 1 \\ \hat{\boldsymbol{\mathcal{B}}}^{(k,1)} \bigcup \cdots \bigcup \hat{\boldsymbol{\mathcal{B}}}^{(k,k-1)}, k \leq q \\ \hat{\boldsymbol{\mathcal{B}}}^{(k,k-q)} \bigcup \hat{\boldsymbol{\mathcal{B}}}^{(k,k-q+1)} \bigcup \cdots \bigcup \hat{\boldsymbol{\mathcal{B}}}^{(k,k-1)}, k > q \end{cases} \tag{53}$$

where the union symbol '$\bigcup$' can make the same predicted locations of different frames appear only once in $\boldsymbol{\Gamma}^{(k)}$.

As shown in Fig. 2(c), the data updating process includes three steps: original data extraction, transmission space freeing, and data vector combining. The first step involves extracting the current LLR data points corresponding to the delay cells where the targets may be located. The second is discarding several data points from $\tilde{\mathbf{L}}_n^{(k)}$ to make space for the data extracted in the first step. Finally, the third step involves the actual process of accommodating the extracted data.

For the sake of the reader, we also provide a simple and typical example presented in Fig. 4. The detailed steps for implementing the data updating process are as follows:

Step 1 – *Original Data Extraction*: Here we extract a part of the original LLR data $\mathbf{L}_n^{(k)}$ of the n-th radar according to the set $\boldsymbol{\Gamma}^{(k)}$, i.e.,

$$\hat{L}_n^{(k)}[m] = \begin{cases} L_n^{(k)}[m], & \text{if } \left| mT_s - \tau_n(\tilde{\boldsymbol{\theta}}) \right| \leq 1/B \\ \text{null}, & \text{else} \end{cases}, \tag{54}$$

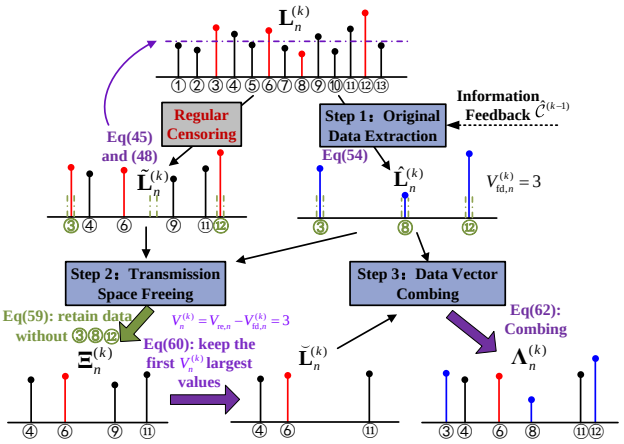

Figure 4. A simple and typical example ($V_{\text{re},n} = 6$) to present the regular censoring and the three steps of data updating: The red lines in the original LLR data $\mathbf{L}_n^{(k)}$ denote the LLR data points of four real targets, while the blue lines in the $\hat{\mathbf{L}}_n^{(k)}$ are the extracted current data points of targets based on the information feedback. It can be seen that the results of regular censoring lack the point ⑧ (see $\tilde{\mathbf{L}}_n^{(k)}$), while the previous detections lack the point ⑥ (see $\hat{\mathbf{L}}_n^{(k)}$). However, thanks to the data updating, we finally succeeded in extracting them simultaneously (see $\boldsymbol{\Lambda}_n^{(k)}$). This is a common phenomenon in the low-SNR scenario and is the reason why our algorithm can work well under communication constraints.

$\forall \tilde{\boldsymbol{\theta}} \in \boldsymbol{\Gamma}^{(k)}, \forall m, n$, where $\hat{L}_n^{(k)}[m] \in \hat{\mathbf{L}}_n^{(k)}$ and

$$\hat{\mathbf{L}}_n^{(k)} \triangleq \left[\hat{L}_n^{(k)}[1], \ldots, \hat{L}_n^{(k)}[m], \ldots, \hat{L}_n^{(k)}[M]\right]^\top. \tag{55}$$

The motivation of (54) is to extract data of the current frame from the delay cells that closely align with predicted locations within the sliding window, specifically those falling within delay resolution $1/B$. Then, we keep the number of non-null number in $\hat{\mathbf{L}}_n^{(k)}$ not more than the upper limit $V_{\text{re},n}$, i.e.,

$$\hat{L}_n^{(k)}[m] = \mathcal{F}(\hat{L}_n^{(k)}[m], V_{\text{re},n}, \hat{\mathbf{L}}_n^{(k)}), \tag{56}$$

$\forall m, n$, where $\mathcal{F}(\cdot)$ is a residual function, defining

$$\mathcal{F}(\nu, \delta, \boldsymbol{\lambda}) = \begin{cases} \nu, & \text{if } \nu \text{ is one of the top } \delta \text{ largest} \\ & \text{elements of the vector } \boldsymbol{\lambda} \\ \text{null}, & \text{otherwise.} \end{cases} \tag{57}$$

Finally, we calculate the number of the extracted non-null data in $\hat{\mathbf{L}}_n^{(k)}$, i.e.,

$$V_{\text{fd},n}^{(k)} = \sum_{m=1}^{M} \mathbb{I}\left(\hat{L}_n^{(k)}[m] \neq \text{null}\right) \tag{58}$$

where $V_{\text{fd},n}^{(k)} \leq V_{\text{re},n}$ due to (56) and the indicator function $\mathbb{I}(\cdot)$ evaluates whether the condition inside the parentheses is true or false: If true, the result is 1; otherwise, it is 0.

Step 2 – *Transmission Space Freeing*: We now have two types of data: the first is the retained LLR data after regular censoring, denoted as $\tilde{\mathbf{L}}_n^{(k)}$, and the other is the extracted original data, represented as $\hat{\mathbf{L}}_n^{(k)}$, which must be ensured for transmission and need to occupy $V_{\text{fd},n}^{(k)}$ positions. The challenge lies in incorporating both types of data, as the non-null data in $\tilde{\mathbf{L}}_n^{(k)}$ may already be at or near transmission saturation due to

limited communication rates (i.e., only $V_{\text{re},n}$ positions are allocated for transmission). Consequently, it becomes necessary to create free transmission space by discarding certain data from $\tilde{\mathbf{L}}_n^{(k)}$ to accommodate the $V_{\text{fd},n}^{(k)}$ non-null data of $\hat{\mathbf{L}}_n^{(k)}$.

Firstly, we extract the LLR data of $\tilde{\mathbf{L}}_n^{(k)}$ outside the corresponding positions of the non-null data in $\hat{\mathbf{L}}_n^{(k)}$, i.e., denoting the corresponding positions as null and extracting other data into a new vector $\mathbf{\Xi}_n^{(k)} \triangleq \left[\Xi_n^{(k)}[1],\ldots,\Xi_n^{(k)}[m],\ldots,\Xi_n^{(k)}[M]\right]^\top$, where

$$\Xi_n^{(k)}[m] = \begin{cases} \text{null}, & \text{if } \hat{L}_n^{(k)}[m] \neq \text{null} \\ \tilde{L}_n^{(k)}[m], & \text{else} \end{cases}, \tag{59}$$

$\forall m,n$. Then, we only keep the first $V_n^{(k)} = V_{\text{re},n} - V_{\text{fd},n}^{(k)}$ largest values of $\mathbf{\Xi}_n^{(k)}$ and discard the remaining smaller elements by assigning them as null, i.e.,

$$\breve{L}_n^{(k)}[m] = \mathcal{F}(\Xi_n^{(k)}[m], V_n^{(k)}, \mathbf{\Xi}_n^{(k)}), \tag{60}$$

$\forall m,n$, where $\breve{L}_n^{(k)}[m]$ is the element of the produced new vector

$$\breve{\mathbf{L}}_n^{(k)} \triangleq \left[\breve{L}_n^{(k)}[1],\ldots,\breve{L}_n^{(k)}[m],\ldots,\breve{L}_n^{(k)}[M]\right]^\top. \tag{61}$$

Now the new produced vector $\breve{\mathbf{L}}_n^{(k)}$ only has $V_n^{(k)}$ non-null numbers, free transmission space for accommodating the $V_{\text{fd},n}^{(k)}$ non-null data of $\hat{\mathbf{L}}_n^{(k)}$ is created.

Step 3 – *Data Vectors Combining*: Eventually, we output the final informative retained data vector $\mathbf{\Lambda}_n^{(k)}$ by incorporating the data vectors $\hat{\mathbf{L}}_n^{(k)}$ and $\breve{\mathbf{L}}_n^{(k)}$, which are respectively produced in **Step 1** and **Step 2**, i.e.,

$$\begin{aligned} \mathbf{\Lambda}_n^{(k)} &= \hat{\mathbf{L}}_n^{(k)} + \breve{\mathbf{L}}_n^{(k)} \\ &\triangleq \left[\Lambda_n^{(k)}[1],\ldots,\Lambda_n^{(k)}[m],\ldots,\Lambda_n^{(k)}[M]\right]^\top \in \mathbb{C}^M, \end{aligned} \tag{62}$$

where

$$\Lambda_n^{(k)}[m] = \begin{cases} \hat{L}_n^{(k)}[m], & \text{if } \hat{L}_n^{(k)}[m] \neq \text{null and } \breve{L}_n^{(k)}[m] = \text{null} \\ \breve{L}_n^{(k)}[m], & \text{if } \hat{L}_n^{(k)}[m] = \text{null and } \breve{L}_n^{(k)}[m] \neq \text{null} \\ \text{null}, & \text{if } \hat{L}_n^{(k)}[m] = \text{null and } \breve{L}_n^{(k)}[m] = \text{null}, \end{cases} \tag{63}$$

$\forall m,n$. It should be noted that the situation when $\hat{L}_n^{(k)}[m] \neq$ null and $\breve{L}_n^{(k)}[m] \neq$ null will not exist because of the opposite definition operation in the first case of (59).

C. Global Decision and Thresholds Setting

At each local station, the retained non-null LLR data after data updating of the k-th ($k = 1,\ldots,K$) frame will be re-quantized and transmitted to the FC for global decision. Here we assume the updated LLR vectors $\{\mathbf{\Lambda}_n^{(k)}\}_{n=1}^N$ can be exactly recovered in the FC without any information loss. Then, the $\{\mathbf{\Lambda}_n^{(k)}\}_{n=1}^N$ can replace the $\{\mathbf{L}_n\}_{n=1}^N$ in (36) and (40). Leveraging the design methodology in Section III-B, the iterative detector for JDL-ECM can be written as

$$\begin{aligned} \hat{\mathbf{\Theta}}^{(k)} &= \{\hat{\boldsymbol{\theta}}_1^{(k)},\ldots,\hat{\boldsymbol{\theta}}_{\hat{P}^{(k)}}^{(k)}\} \\ \text{with } \ \hat{\boldsymbol{\theta}}_p^{(k)} &= \arg\max_{\boldsymbol{\theta}\in\mathcal{G}} \mathcal{Z}_p^{(k)}(\boldsymbol{\theta}) \\ \text{s.t. } \max_{\boldsymbol{\theta}\in\mathcal{G}} \mathcal{Z}_p^{(k)}(\boldsymbol{\theta}) &\geq \psi'(\varrho_p(\boldsymbol{\theta})),\ p \leq P_{\max}. \end{aligned} \tag{64}$$

In (64), the $\mathcal{Z}_p^{(k)}(\boldsymbol{\theta})$ is the p-th updated LLR function at the k-th frame and satisfies $\mathcal{Z}_1^{(k)}(\boldsymbol{\theta}) = \mathcal{Z}^{(k)}(\boldsymbol{\theta})$ if $p = 1$ and

$$\mathcal{Z}_p^{(k)}(\boldsymbol{\theta}) = \mathcal{Z}^{(k)}(\boldsymbol{\theta}) - \sum_{n=1}^{N}\sum_{i=1}^{p-1} \mathcal{X}_{n,i}^{(k)}\left(\boldsymbol{\theta}, \hat{\boldsymbol{\theta}}_i^{(k)}\right), \text{if } p \geq 2, \tag{65}$$

where

$$\mathcal{Z}^{(k)}(\boldsymbol{\theta}) = \sum_{n=1}^{N} \Lambda_n^{(k)}[\lceil \tau_n(\boldsymbol{\theta})/T_s \rceil], \boldsymbol{\theta} \in \mathcal{G}, \tag{66}$$

and

$$\mathcal{X}_{n,p}^{(k)}\left(\boldsymbol{\theta}; \hat{\boldsymbol{\theta}}_p^{(k)}\right) = \begin{cases} \Lambda_n^{(k)}[\lceil \tau_n(\boldsymbol{\theta})/T_s \rceil], \boldsymbol{\theta} \in \mathbb{B}_n\left(\boldsymbol{\theta}; \hat{\boldsymbol{\theta}}_p^{(k)}\right) \\ 0, \text{others}. \end{cases} \tag{67}$$

The detection threshold $\psi'(\varrho_p(\boldsymbol{\theta}))$ will be employed under the situation when there are $\varrho_p(\boldsymbol{\theta})$ LLR values superimposed in $\mathcal{Z}_p^{(k)}(\boldsymbol{\theta})$. The positive integer $\varrho_p(\boldsymbol{\theta})$ satisfies $\varrho_1(\boldsymbol{\theta}) = \sum_{n=1}^N \mathbb{I}\left(\Lambda_n^{(k)}[\lceil \tau_n(\boldsymbol{\theta})/T_s \rceil] \neq \text{null}\right)$ if $p = 1$ and

$$\begin{aligned} \varrho_p(\boldsymbol{\theta}) = &\sum_{n=1}^{N} \mathbb{I}\left(\Lambda_n^{(k)}[\lceil \tau_n(\boldsymbol{\theta})/T_s \rceil] \neq \text{null}\right) \\ &- \sum_{n=1}^{N}\sum_{i=1}^{p-1} \mathbb{I}\Big(\mathcal{X}_{n,i}^{(k)}(\boldsymbol{\theta}, \hat{\boldsymbol{\theta}}_i^{(k)}) \neq \text{null} \\ &\quad \text{and } \mathcal{X}_{n,i}^{(k)}(\boldsymbol{\theta}, \hat{\boldsymbol{\theta}}_i^{(k)}) \neq 0\Big), \text{if } p \geq 2. \end{aligned} \tag{68}$$

Remark 7. In other words, there are N possibilities for the threshold, i.e., $\psi'(\varrho), \varrho = 1,\ldots,N$. We can construct a vector $\boldsymbol{\psi}' = [\psi'(1),\ldots,\psi'(N)]$ to prepare for the threshold selecting. It is worth noting that it is pretty difficult or even impossible to obtain the analytical distribution of $\mathcal{Z}_p^{(k)}(\boldsymbol{\theta})$ due to the complex function relation for these Gaussian random variables. To ensure the global CFAR property, we adopt the Monte Carlo simulation and the target-free experimental data to compute each detection threshold of $\boldsymbol{\psi}'$ in the simulation analysis and experimental tests, respectively.

Then, the iterative detector for JDL-ECM in (64) will extract the targets one by one, and the corresponding estimated target location will be added to the estimated locations set $\hat{\mathbf{\Theta}}^{(k)}$ step by step. When the detection procedure is finished, i.e., the maximum value does not exceed its corresponding threshold or p exceeds $P_{\max}$, then the estimated number $\hat{P}^{(k)} = p-1$ and location set $\hat{\mathbf{\Theta}}^{(k)}$ can be obtained. Next, the target velocities will be estimated at the FC by utilizing the relationships of the output estimated locations in different frames. If $k = 1$, then denote $\hat{\boldsymbol{v}}_p^{(k)} = \mathbf{0}$. If $k \geq 2$, given the current estimated location set $\hat{\mathbf{\Theta}}^{(k)}$, we leverage the design methodology of the Hungarian algorithm [65] to realize the association of

targets between the current and the previous frames, and then calculate the estimated velocities. Specifically, for the p-th estimated location $\hat{\boldsymbol{\theta}}_p^{(k)} \in \hat{\boldsymbol{\Theta}}^{(k)}$ at the k-th frame its corresponding velocity can be calculated as follows

$$\begin{aligned}\hat{\boldsymbol{v}}_p^{(k)} = &\left(\hat{\boldsymbol{\theta}}_p^{(k)} - \underset{\hat{\boldsymbol{\theta}}^{(i)}\in\hat{\boldsymbol{\Theta}}^{(i)}}{\arg\min} \left\|\hat{\boldsymbol{\theta}}_p^{(k)} - \hat{\boldsymbol{\theta}}^{(i)}\right\|\right)/\big((k-i)T_{\text{frame}}\big)\\ \text{s.t.} &\min_{\hat{\boldsymbol{\theta}}^{(i)}\in\hat{\boldsymbol{\Theta}}^{(i)}} \left\|\hat{\boldsymbol{\theta}}_p^{(k)} - \hat{\boldsymbol{\theta}}^{(i)}\right\| \le \zeta,\ p=1,\ldots,\hat{P}^{(k)},\ k\ge 2,\end{aligned} \tag{69}$$

where $i = 1, \ldots, k-1$ and ζ is the set distance threshold. It should be noted that the index of the previous frame "i" will be selected in descending order, i.e., from $k-1$ to 1, and the process of (69) will terminate once the estimated velocity $\hat{\boldsymbol{v}}_p^{(k)}$ has been determined.

Remark 8. To estimate velocities in the distributed monopulse radar system, which neglects Doppler shifts, target estimated locations across frames are utilized. As targets may not be fully detected in every frame, estimated locations from the current and the previous $k-1$ frame may be insufficient. Thus, the system traverses earlier frames (from $k-1$ to 1) to associate the previous and current estimated locations, enabling velocity estimation for the current frame. Assuming the FC does not know if target velocities are fixed, estimated velocities calculated from adjacent frames are prioritized to ensure accurate LLR data retention for the $(k+1)$-th frame under the censoring framework. This approach also indicates that the JDL-ECM is also adaptable for the JDL of moving targets with variable velocities under communication constraints.

Finally, the estimated locations and velocities at the k-th frame will be added to the set

$$\hat{\boldsymbol{\mathcal{C}}}^{(k)} = \{(\hat{\boldsymbol{\theta}}_1^{(k)}, \hat{\boldsymbol{v}}_1^{(k)}), \ldots, (\hat{\boldsymbol{\theta}}_{\hat{P}^{(k)}}^{(k)}, \hat{\boldsymbol{v}}_{\hat{P}^{(i)}}^{(k)})\}, \tag{70}$$

which will be fed back to each radar to update the set $\boldsymbol{\Gamma}^{(k+1)}$ for the data updating of the next frame. The overall procedure is summarized in Algorithm 1.

Algorithm 1 Implementation of the proposed JDL-ECM algorithm

provide The inspected location region $\mathcal{G}$ including $Q_{\mathcal{G}}$ grids, limited communication rate Υ_n, quantized bit depth γ, detection threshold vector $\boldsymbol{\psi}'$, assumed upper bound of the prospective targets number $P_{\max}$, the original LLR data $\mathbf{L}_n^{(k)}$ $(n = 1, \ldots, N)$, original feedback set $\hat{\boldsymbol{\mathcal{C}}}^{(k)} = \varnothing$, the estimated target number $\hat{P}^{(k)} = 0$, the previous location sets $\hat{\boldsymbol{\Theta}}^{(i)}, i = 1, \ldots, k-1$, the distance threshold ζ and the union of the prediction sets $\boldsymbol{\Gamma}^{(k)}$.
if $k = 1$ **then**
  Compute $\mathcal{Z}^{(k)}(\boldsymbol{\theta})$ from (66), (62), and (61), with $\hat{\mathbf{L}}_n^{(k)} = \varnothing$ and $V_{\text{fd},n}^{(k)} = 0$
else
  Compute $\mathcal{Z}^{(k)}(\boldsymbol{\theta})$ from (66), (62), (61) and (55)
end if
for $p = 1, \ldots, P_{\max}$ **do**
  Compute $\mathcal{Z}_p^{(k)}(\boldsymbol{\theta})$ and $\varrho_p(\boldsymbol{\theta})$ from (65) and (68)
  if $\max_{\boldsymbol{\theta}\in\mathcal{G}}\ \mathcal{Z}_p^{(k)}(\boldsymbol{\theta}) \ge \psi'(\varrho_p(\boldsymbol{\theta}))$ **then**
    Compute $\hat{\boldsymbol{\theta}}_p^{(k)} = \underset{\boldsymbol{\theta}\in\mathcal{G}}{\arg\max}\ \mathcal{Z}_p^{(k)}(\boldsymbol{\theta})$ and $\hat{P}^{(k)} = p$
  else
    break
  end if
end for
for $p = 1, \ldots, \hat{P}^{(k)}$ **do**
  Compute $\hat{\boldsymbol{v}}_p^{(k)} = \mathbf{0}$
  if $k \ge 2$ **then**
    for $j = 1, \ldots, k-1$ **do**
      Compute $i = k - j$
      if $\min_{\hat{\boldsymbol{\theta}}^{(i)}\in\hat{\boldsymbol{\Theta}}^{(i)}} \left\|\hat{\boldsymbol{\theta}}_p^{(k)} - \hat{\boldsymbol{\theta}}^{(i)}\right\| \le \zeta$ **then**
        Compute $\hat{\boldsymbol{v}}_p^{(k)}$ from (69)
        break
      end if
    end for
  end if
  Compute $\hat{\boldsymbol{\mathcal{C}}}^{(k)} = \hat{\boldsymbol{\mathcal{C}}}^{(k)} \cup \{(\hat{\boldsymbol{\theta}}_p^{(k)}, \hat{\boldsymbol{v}}_p^{(k)})\}$
end for
return $\hat{P}^{(k)}$ and $\hat{\boldsymbol{\mathcal{C}}}^{(k)}$, which will be fed back to each local station to update $\boldsymbol{\Gamma}^{(k+1)}$ from (53), (52), and (51)

D. Discussion

1) Computational Analysis: Corresponding to Section III-C1, the JDL-UCR employing low-dimensional solution requires at least $\mathcal{O}\big(NM^3 + NPQ_{\mathcal{G}}\big)$ flops. In addition to these, the JDL-ECM algorithm also needs to perform regular censoring and data updating to obtain updated LLR data. The computational load of the regular censoring at each station is $\mathcal{O}\big(M\big)$ flops. The data updating process includes original data extraction, transmission space freeing, and data vector combining, which incur the costs of $\mathcal{O}\big(PM\big)$ flops (assuming that P targets are detected and estimated in the previous q frames), $\mathcal{O}\big(M\log_2(M)\big)$ flops, and $\mathcal{O}\big(M\big)$ flops, respectively. Besides, the calculation of location prediction sets in (51)-(53) requires $\mathcal{O}\big(q\big)$, while the velocity estimation in (69) costs at least $\mathcal{O}\big(P^2\big)$ flops. Therefore, considering N stations, the total cost for the JDL-ECM is at least $\mathcal{O}\big(N(PM+M\log_2(M))\big)+\mathcal{O}\big(NM^3+NPQ_{\mathcal{G}}+q+P^2\big)$ flops.

2) Communication Rates Analysis: Corresponding to Section III-C2, in this case, the non-null data of the final updated vector $\boldsymbol{\Lambda}_n^{(k)}$ in (62) will also be re-quantized by $\gamma = \gamma_1 + \gamma_2$ bits per point before being transmitted to the FC within the T_{tran} time. Then the actual communication rates per second between the n-th radar and the FC, under communication constraints (CC), can be calculated by

$$W_n^{\text{CC}} = \left(\sum_{m=1}^{M} \mathbb{I}\left(\Lambda_n^{(k)}[m] \ne \text{null}\right)\gamma\right)/T_{\text{tran}}\ \text{bps}. \tag{71}$$

Remark 9. Although this paper primarily focuses on distributed monopulse radars, the proposed JDL-ECM algorithm is also extensible to distributed multi-pulse radar systems by incorporating Doppler shifts considerations. For instance, by integrating with the signal model presented in [39], the algorithm can also effectively censor transmitted delay-Doppler LLR data through the utilization of location and velocity feedback from the FC. Subsequently, the filtered LLR data

Table III
SIMULATION SYSTEM PARAMETERS

Parameter	Value
Number of Radars, N	9
Carrier Frequency, $\{f_c^n\}_{n=1}^N$	75 : 0.5 : 79 GHz
Bandwidth, B	150 MHz
Sampling Interval, T_s	0.2 μs
Modulated Duration, T	300 μs
PRI, T_{pri}	300 μs
Frame Duration, T_{frame}	50 ms
Transmission Duration, T_{tran}	20 ms
Sample Points, M	1500
Range Bin	1 m
Distance Threshold, ζ	5 m
Inter-Element Spacing, Δ_g	1 m
Noise Variance, σ_w^2	1
LLR Data Quantization Bits, γ ($\gamma_1+\gamma_2$)	80 ($16+64$) bits
Quantization Bits of Feedback Data, γ_3	160 bits / Frame

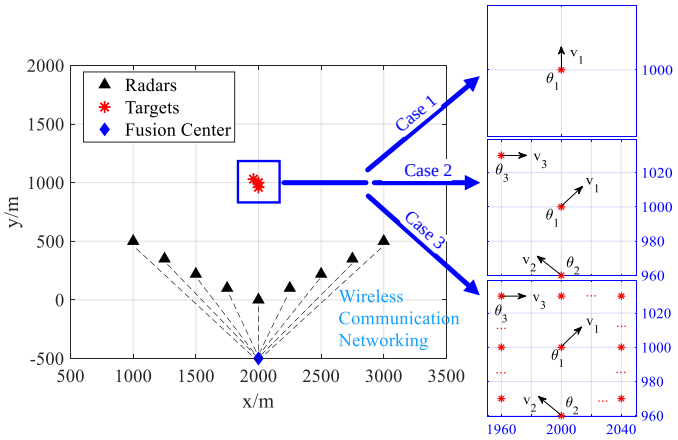

Figure 5. The 3 km × 2.5 km plane involving 9 radars and an FC. The radars are placed at $\boldsymbol{x}_1 = (1000, 500)$ m, $\boldsymbol{x}_2 = (1250, 350)$ m, $\boldsymbol{x}_3 = (1500, 220)$ m, $\boldsymbol{x}_4 = (1750, 100)$ m, $\boldsymbol{x}_5 = (2000, 0)$ m, $\boldsymbol{x}_6 = (2250, 100)$ m, $\boldsymbol{x}_7 = (2500, 220)$ m, $\boldsymbol{x}_8 = (2750, 350)$ m, and $\boldsymbol{x}_9 = (3000, 500)$ m.

can be transmitted to the FC, enabling high-performance target detection and precise estimation of locations/velocities while adhering to communication constraints.

V. PERFORMANCE ASSESSMENT

A. Simulation Analysis

In this section, simulation analyses are provided to demonstrate the performance of the proposed JDL-ECM algorithm. As an implementation example, we consider a distributed monopulse radar system employing actual FMCW waveforms [66], with the parameters in Table III and the geometry in Fig. 5. Three cases are considered: Case 1 is the single moving target case where Target 1 is initially located at $\boldsymbol{\theta}_1 = (2000, 1000)$ m with velocity $\boldsymbol{v}_1 = (0, 20)$ m/s; Case 2 involves three moving targets where Targets 1, 2, and 3 are initially located at $\boldsymbol{\theta}_1 = (2000, 1000)$ m, $\boldsymbol{\theta}_2 = (2000, 960)$ m, and $\boldsymbol{\theta}_3 = (1960, 1030)$ m, with velocities $\boldsymbol{v}_1 = (20, 20)$ m/s, $\boldsymbol{v}_2 = (-20, 20)$ m/s and $\boldsymbol{v}_3 = (0, 20)$ m/s, respectively; Case

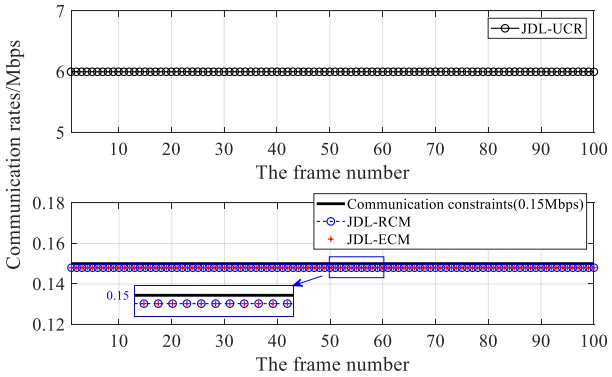

Figure 6. The relationship between the communication rates of a single station and the frame number.

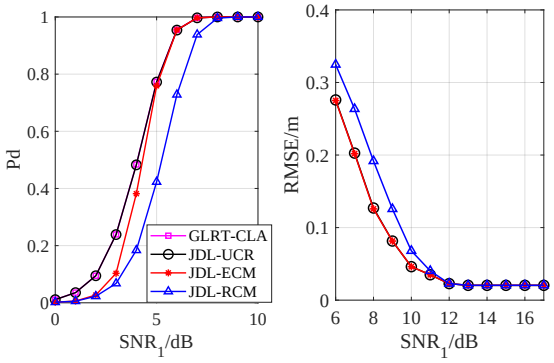

Figure 7. Single Moving Target Performance: P_d (left) and RMSE in the position estimate (right) of Target 1 versus SNR_1 when $q = 3$.

3 includes P ($P > 3$) targets, in addition to Targets 1, 2, and 3 of Case 2, the locations of $P-3$ targets are randomly selected around the three moving targets. To reduce the amount of grid search, every 50 frames, all moving targets will be adjusted to the velocities completely opposite to the previous 50 frames. Therefore, all targets belong to the inspected location region $\mathbb{Y} = [1950, 2050] \times [950, 1050]$ m^2 with $\Delta_g = 1$ m.

The probability of valid target detection (P_d) and the localization root mean square error (RMSE) are used as metrics to assess the detection and localization performance [36]. The global false alarm rate is set as $P_{fa} = 10^{-3}$, and the results are obtained by averaging over $K_{\max} = 10000$ frames. In the following, three benchmarks are considered for comparison:

(a) GLRT clairvoyant detector (GLRT-CLA): the GLRT detector with known location of target [26], [67].
(b) JDL-UCR algorithm: the algorithm proposed in Section III when the system under no communication constraints.
(c) JDL with regular censoring method (JDL-RCM): the JDL-ECM algorithm without considering the information feedback, i.e., $\mathbf{\Gamma}^{(k)} = \varnothing, \forall k$ and ignoring the original data extraction step in the data updating.

1) Single Moving Target Simulation (Case 1): Traffic Load and Performance Comparison: According to the calculation of (42), the traffic load of JDL-UCR is $W_n^{\text{UCR}} = 6$ Mbps. Here we consider that the communication constraints between each radar and the FC are $\Upsilon_n = 0.15$ Mbps, $\forall n$, i.e., the corresponding data retaining percentage after censoring can

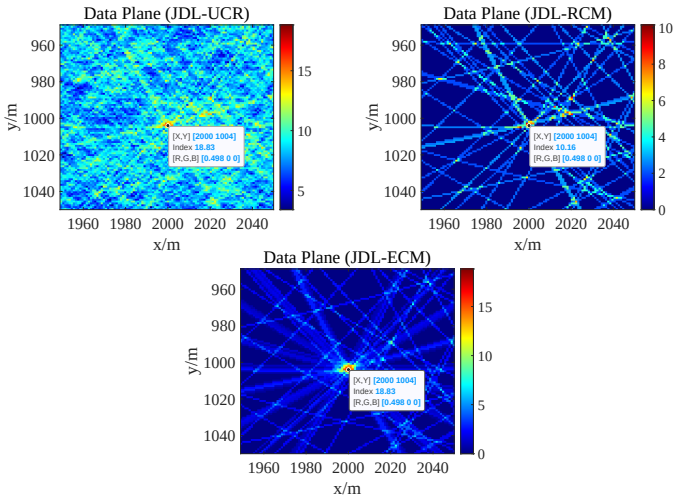

Figure 8. Output data planes $\mathcal{D}_1(\boldsymbol{\theta})$ in (39) of the JDL-UCR (top-left), $\mathcal{Z}_1(\boldsymbol{\theta})$ in (65) of the JDL-RCM (top-right) and JDL-ECM (bottom) when $\mathrm{SNR}_1 = 7$ dB and $k = 5$.

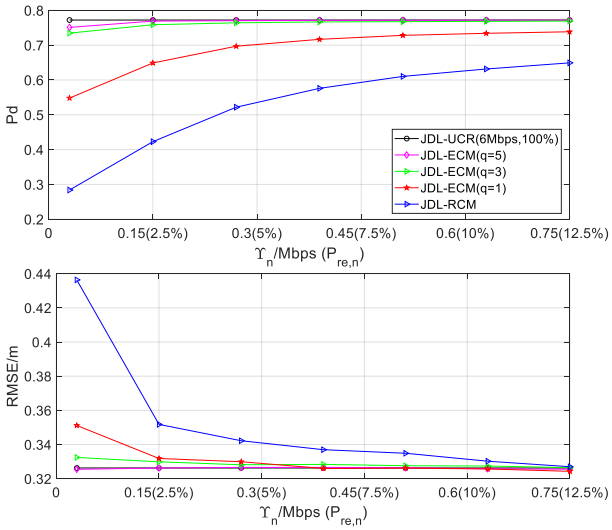

Figure 9. Single Moving Target Performance: $\mathrm{P_d}$ (top) and RMSE in the position estimate (bottom) of Target 1 versus the limited communication rates Υ_n (or the corresponding data retaining percentage $\mathrm{P_{re},}_n$) with different sliding window length q when $\mathrm{SNR}_1 = 5$ dB.

be calculated using (43) as $\mathrm{P_{re},}_n = 2.5\%$, and the sliding window length of information feedback is set as $q = 3$. Firstly, we illustrate the relationship between the communication rates of a single station and the frame number in Fig. 6. It can be seen that the communication rates W_n^{CC} required by the JDL-ECM or the JDL-RCM can always meet the communication constraints of 0.15 Mbps given by the system at the expense of reduced detection and localization performance, which will be investigated in the upcoming examples.

Then, the detection and localization performance of different methods are shown in Fig. 7. We can first observe that the $\mathrm{P_d}$ achieved by the devised JDL-UCR under no communication constraints closely aligns with the GLRT-CLA. This initial comparison serves to illustrate the effectiveness of the JDL-UCR in the target detection within an inspected location region. The proposed JDL-ECM algorithm performs slightly worse than the JDL-UCR but incurs only a small communication cost, which confirms its capability to accurately detect and localize targets even under unfavorable communication conditions. Compared with the JDL-ECM, the JDL-RCM exhibits worse performance. To illustrate this phenomenon, the output data planes of these algorithms (i.e., the $\mathcal{D}_p(\boldsymbol{\theta})$ in (39) for the JDL-UCR over $\mathbb{Y}$, the $\mathcal{Z}_p(\boldsymbol{\theta})$ in (65) for the JDL-RCM or JDL-ECM over $\mathbb{Y}$, and $p = 1$ here) in a single snapshot are reported in Fig. 8, when $\mathrm{SNR}_1 = 7$ dB and $k = 5$. It can be seen that the JDL-RCM obtains a lower maximum data value, i.e., not all of the informative data are retained effectively for data fusion at the FC. However, the JDL-ECM achieves the maximum value with the JDL-UCR algorithm. This phenomenon reveals that the JDL-ECM can effectively retain the 9-path informative moving-target data thanks to the information feedback, correct location prediction, and efficient data censoring.

2) Single Moving Target Simulation (Case 1): Impact of Limited Communication Rates Υ_n and Sliding Window Length q: In this subsection, we consider the impact of the limited communication rates Υ_n on the detection and localization performance under low-SNR environment when $\mathrm{SNR}_1 = 5$ dB, which is shown in Fig. 9. It can be seen that the performance of the proposed JDL-ECM algorithm improves as the Υ_n are relaxed (i.e., the data retaining percentage $\mathrm{P_{re},}_n$ is increasing), and the JDL-RCM also has the same regular phenomenon. However, the JDL-ECM has much higher performance, which indicates its robustness in the case of extremely limited communication rates. The reason is that the JDL-ECM utilizes the data updating to make the transmitted data more informative, thus improving the global performance, while the performance of the JDL-RCM only depends on the increase of the data retaining percentage. Besides, we also consider the impact of the sliding window length q of information feedback on the detection and localization performance. We can see that the performance of the proposed JDL-ECM increases with q, and it is close to the JDL-UCR algorithm when it reaches 5.

3) Simulations of Multiple Moving Targets (Cases 2 and 3): Verification of the Effectiveness in Addressing Multi-target Cases: Based on the settings and results of the previous single-target case, here we will verify the effectiveness of the proposed JDL-ECM algorithm in addressing the cases of multiple moving targets. For Case 2, we assume the ratio of the SNRs of the three targets as $\mathrm{SNR}_1 : \mathrm{SNR}_2 : \mathrm{SNR}_3 = 1 : 0.64 : 0.25$, while setting $\Upsilon_n = 0.15$ Mbps ($\mathrm{P_{re},}_n = 2.5\%$) and $q = 5$. Then from the $\mathrm{P_d}$ and RMSE results in Fig. 10, we can see all the targets are effectively detected and localized by all algorithms. Similar to the single-target simulation, the JDL-ECM performs slightly worse than the JDL-UCR but incurs only a small communication cost, and also outperforms JDL-RCM while maintaining similar communication costs. Next, the real and estimated target locations within 50 frames when $\mathrm{SNR} = 9$ dB are shown in Fig. 11. It can be seen that the estimated locations of the JDL-ECM algorithm are always consistent with the JDL-UCR. These phenomenons verify the effectiveness of efficient censoring method, which can efficiently retain the data of multiple moving targets from different local radars.

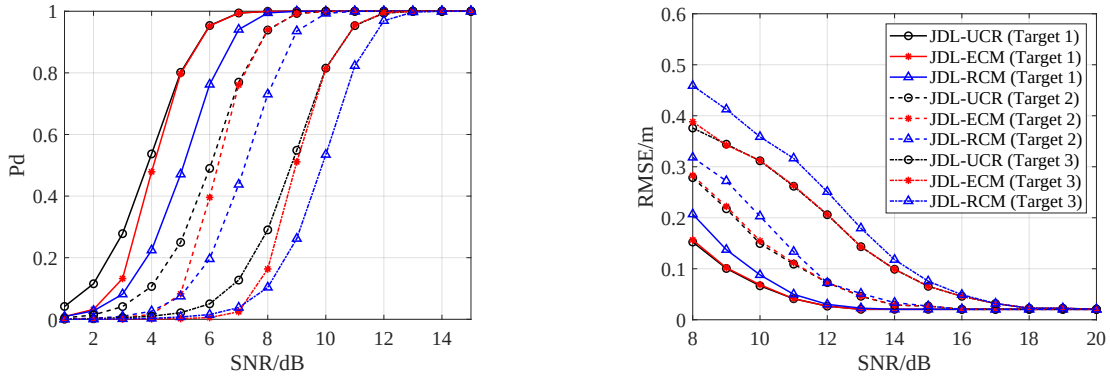

Figure 10. Multiple Moving Targets Performance: $\mathrm{P_d}$ (left) and RMSE in the position estimate (right) of all targets versus SNR_1 when $\Upsilon_n = 0.15$ Mbps ($\mathrm{P}_{\mathrm{re},n} = 2.5\%$) and $q = 5$. It should be noted that the JDL-UCR incurs the communication rates of 6 Mbps, while the JDL-ECM and JDL-RCM each incurs 0.15 Mbps here.

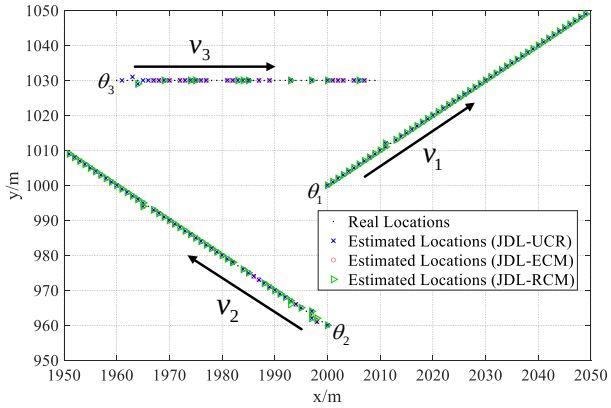

Figure 11. The real and estimated target locations by using JDL-UCR, JDL-ECM, and JDL-RCM algorithms within 50 frames when SNR = 9 dB.

In Case 3, we assume the ratios between the SNRs of other targets and that of Target 1 are $\mathrm{SNR}_p/\mathrm{SNR}_1 \in (0, 4]$, for $p = 2, \ldots, P$, while setting $\mathrm{SNR}_1 = 6$ dB and $q = 5$. Then, Fig. 12 shows the $\mathrm{P_d}$ and RMSE results of Target 1 versus the number of targets P with different Υ_n. It can be seen that the JDL-ECM exhibits superior performance in comparison to the JDL-RCM, although both of them will lose some performance with an increasing number of targets. Additionally, their performance is also affected by the limited communication rates Υ_n: with higher rates yielding better performance. When $\Upsilon_n = 0.15$ Mbps (i.e., $\mathrm{P}_{\mathrm{re},n} = 2.5\%$) and within a range of up to 11 targets, the JDL-ECM achieves performance nearly equivalent to JDL-UCR, which requires a cost of 6 Mbps. Besides, when $\Upsilon_n = 0.06$ Mbps (i.e., $\mathrm{P}_{\mathrm{re},n} = 1\%$) and $P = 11$, the JDL-ECM will lose performance. For the reason, it is because the JDL-ECM prioritizes the retaining of data from other stronger targets at a very limited communication rate, without enough space to accommodate the data from Target 1 for all paths. These findings show that communication constraints impact target detection and localization, while also highlighting the effectiveness of the proposed JDL-ECM in handling multiple moving targets scenarios with minimal communication costs, especially compared to JDL-UCR.

Table IV
EXPERIMENTAL SYSTEM PARAMETERS

Parameter	**Value**
Number of Radars, N	5
Carrier Frequency, $\{f_c^n\}_{n=1}^N$	$76:1:80$ GHz
Bandwidth, B	480 MHz
Sampling Interval, T_s	0.2 μs
Modulated Duration, T	51.2 μs
PRI, T_pri	160 μs
Frame Duration, T_frame	50 ms
Transmission Duration, T_tran	20 ms
Maximum Unambiguous Distance	80 m
Sample Points of Each PRI, M	256
The Number of PRI in One Frame	128
Range Bin	0.3125 m
The Sliding Window Length, q	5
Inter-Element Spacing, Δ_g	0.3125 m
LLR Data Quantization Bits, γ ($\gamma_1 + \gamma_2$)	80 ($16 + 64$) bits
Quantization Bits of Feedback Data, γ_3	160 bits / Frame
Global False Alarm Rate, $\mathrm{P_{fa}}$	10^{-3}

B. Experimental Tests

In this study, the real data obtained from five distributed millimeter-wave FMCW radars are employed to evaluate the effectiveness of the proposed JDL-ECM algorithm. These radars are utilized to accurately determine the positions of targets in an open field, which exhibits a nearly homogeneous background. To be specific, Fig. 13 shows the photos of experimental devices[7], ground, and scenarios, where Scenario 1 considers a single stationary human target with or without a corner reflector in his hands (Target A or B), and Scenario 2 considers two stationary targets placed one behind the other (Targets C and D). Table IV illustrates the parameters of the FMCW radars, respectively. The radars are designed

[7]The FMCW radars we used are commercially available from Texas Instruments, a leading manufacturer in this field. These devices are widely adopted in various real-world applications, ensuring that our experimental setup is both relevant and realistic. While it is true that any commercial device may have intrinsic limitations, we selected these sensors precisely because they reflect the operational conditions and performance that can be expected in practical deployments.

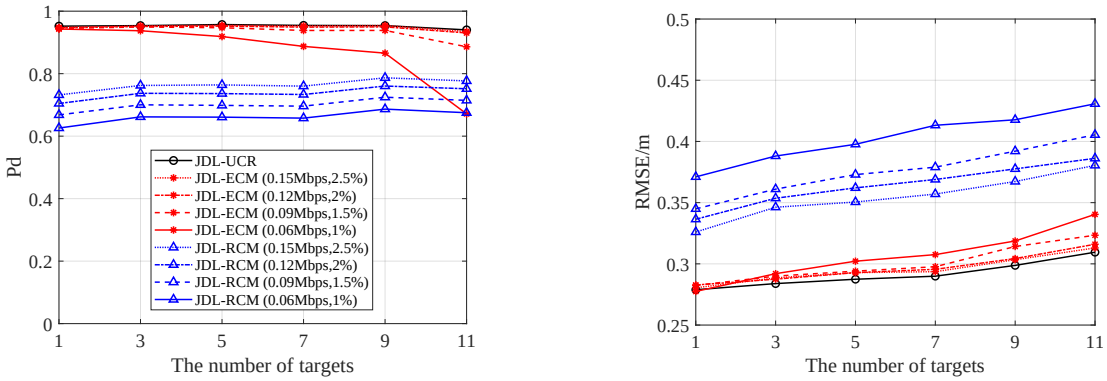

Figure 12. Multiple Moving Targets Performance: $\mathrm{P_d}$ (left) and RMSE in the position estimate (right) of Target 1 versus the number of targets with different Υ_n ($\mathrm{P}_{\mathrm{re},n}$) when $\mathrm{SNR}_1 = 6$ dB and $q = 5$. It is worth mentioning that the JDL-UCR requires a cost of 6 Mbps, while the JDL-ECM and JDL-RCM each incurs a cost of the corresponding Υ_n Mbps.

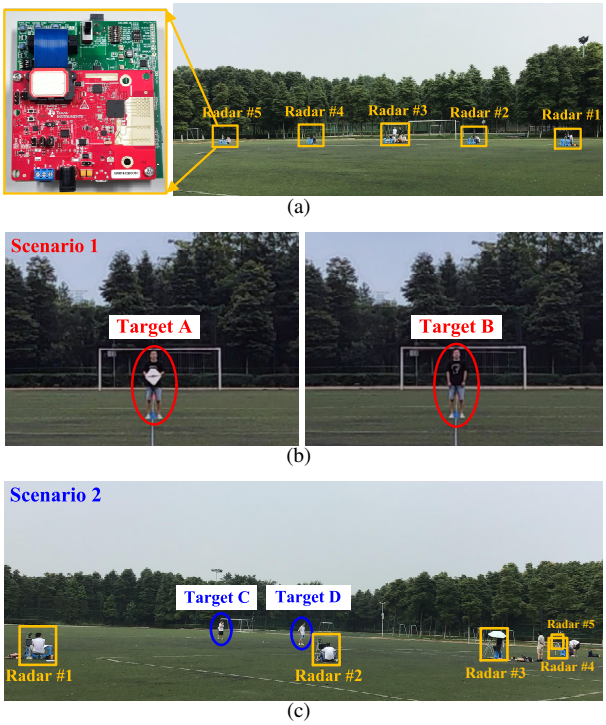

Figure 13. Experimental devices, ground, and scenarios: (a) The distributed FMCW radars are placed on an empty football ground. (b) Scenario 1: a stationary target with or without a corner reflector in his hands (Target A or B, placed alone). (c) Scenario 2: two stationary targets (Target C and D, placed simultaneously).

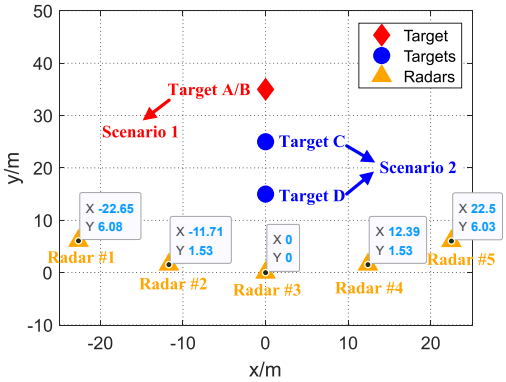

Figure 14. The geometric relationship between distributed layout FMCW radars and the targets of two scenarios.

with a sufficiently wide beamwidth, enabling them to cover the surveillance area in an almost omnidirectional manner. This configuration ensures that the target within the area can be simultaneously illuminated by the five radars. Due to hardware constraints, each radar operates in receiving its own echo by frequency-division duplexing, i.e., $\{f_c^n\}_{n=1}^N = 76 : 1 : 80$ GHz, thus each FMCW radar contributes one path and a five-path distributed FMCW radars system has been created. Although the actual FMCW radar devices transmit multiple PRIs in a frame and given the stationary targets in the experiments, we directly extract the zero-frequency data of the delay- and Doppler-dimensional data plane as the delay-dimensional observations. Additionally, given that the range bin width is 0.3125 m, humans in our experiments do not span multiple bins. Consequently, they do not exhibit characteristics typical of extended targets.

Fig. 14 shows the geometric relationships between the distributed FMCW radars and the targets of two scenarios: Five radars are located at $(-22.65, 6.08)$ m, $(-11.71, 1.53)$ m, $(0, 0)$ m, $(12.39, 1.53)$ m, and $(22.5, 6.03)$ m, respectively; Target A or B is located at $(0, 35)$ m; Targets C and D are simultaneously located at $(0, 25)$ m and $(0, 15)$ m. To create a ground-truth, a standard rangefinder is utilized to determine the Cartesian coordinates of both the radars and the stationary target. The experimental data are processed offline after being recorded, and the noise power and detection thresholds are estimated and calculated by analyzing 1000 frames of target-free experimental scene data. Based on the parameters shown in Table IV, the communication rates of the JDL-UCR algorithm between the n-th local radar and the FC can be calculated by $W_n^{\mathrm{UCR}} = M\gamma/T_{\mathrm{tran}} = 1.0240$ Mbps.

1) Scenario 1: Single target placed with or without a corner reflector: In this scenario, we assume the data retaining percentage $\mathrm{P}_{\mathrm{re},n} = 2.5\%$, which means the transmitted data of JDL-ECM or JDL-RCM can be compressed to 2.5% of that of JDL-UCR and the communication constraints can be limited to $\Upsilon_n = 0.0256$ Mbps. It should be noted that the corner

Table V
THE MULTI-FRAME RESULTS FOR ALL CONSIDERED ALGORITHMS WITH DIFFERENT TARGETS IN DIFFERENT SCENARIOS

		Results / Algorithms / Metrics	JDL-UCR	JDL-RCM	JDL-ECM
Scenario 1 (500 frames)	Target A	P_d	0.9980	0.9980	0.9980
		RMSE (m)	0.2545	0.2495	0.2513
	Target B	P_d	**0.6260**	**0.4580**	**0.6140**
		RMSE (m)	0.3461	0.3354	0.3278
		W_n(Mbps)	1.0240	0.0256	0.0256
Scenario 2 (480 frames)	Target C	P_d	**0.5354**	**0.3646**	**0.5333**
		RMSE (m)	0.2835	0.3125	0.2887
	Target D	P_d	1.0000	1.0000	1.0000
		RMSE (m)	0.2341	0.2357	0.2319
		W_n(Mbps)	1.0240	0.0410	0.0410

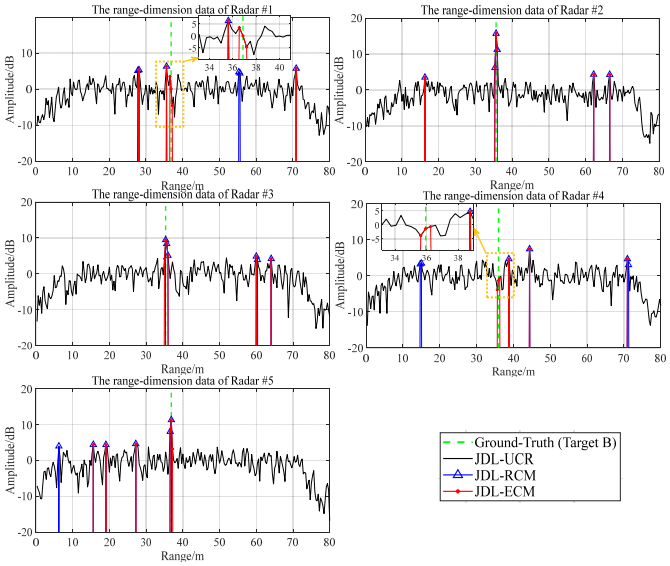

Figure 15. The delay-dimensional data from various radars after normalizing noise power in the 26-th frame during the probing of Target B in Scenario 1. In the orange dashed rectangles of these figures, we can see the proposed JDL-ECM succeeded in retaining the small amplitudes of Target B.

reflector will bring high RCS [68], therefore the echoes of Target B are expected to be weaker than Target A (i.e., here we can treat Target A and B as a strong and a weak target.).

Firstly, the 500-frame statistical results of Scenario 1 in Table V report that all of the three algorithms can achieve almost the same high performance when detecting the strong Target A; meanwhile, all of the actual communication rates are consistent with the settings, i.e., the JDL-RCM and JDL-ECM incur low communication rates but reach almost the same high performance with the JDL-UCR utilizing full data sets. Then, same as expected, the detection and localization performance of all of the algorithms drops a lot when detecting the weak Target B (i.e., the one without the corner reflector). Especially, the detection performance gap between the JDL-RCM and JDL-UCR is widened in this case, but the proposed JDL-ECM algorithm can still maintain a very close performance to that of the JDL-UCR, which reveals that the JDL-ECM is particularly robust especially in low-SNR cases.

To illustrate the reason, Figs. 15 and 16 show the delay-dimensional echoes of different radars at the 26-th frame and the detailed detection results of the total 500 frames. From Fig. 16 we know that the JDL-UCR and JDL-ECM successfully detected the target at the 26-th frame whereas the JDL-RCM algorithm failed. Back to Fig. 15, we can see the JDL-UCR employs completed delay-dimensional data, while the JDL-RCM and JDL-ECM only reserve several prominent peaks to satisfy the setting communication constraints. It is noteworthy that the JDL-ECM retains echo data from the range bin where the actual target is located, a capability not exhibited by the JDL-RCM algorithm in the data of radar 1 and 4 (refer to the orange dashed rectangles in Fig. 15), despite the relatively small amplitude of this range bin. This is because the target is detected in the previous $q = 5$ frames and its estimated location is fed back to take part in the data updating at the following frames. Therefore, compared with the JDL-RCM, the proposed JDL-ECM can have more informative echo data for data fusion, thus achieving higher detection performance under limited communication rates.

2) Scenario 2: Two targets placed one behind the other: With the increase in the number of targets to 2 in this scenario, we also raise the data retaining percentage to $P_{re,n} = 4\%$, and the communication constraints can be limited to $\Upsilon_n = 0.0410$ Mbps. It should be noted that Targets C and D are simultaneously placed, and the distance between Target C and each radar is farther than that between Target D and each radar, and from the perspective of Radar 3, Target C will be blocked by Target D. Therefore, the scenario is similar to Scenario 1 but with the different characteristics regarding path attenuation and object occlusion, and the amplitudes of Target C are also expected to be weaker than Target D.

We report the results of Scenario 2 in Table V and Fig. 17, and observe better detection performance for Target D than for Target C, as expected. The performance gap between the JDL-RCM and JDL-UCR also exists, but the proposed JDL-ECM still keeps close to the JDL-UCR, including both detection and localization performance. All of the actual communication rates are also consistent with the settings. Besides, Fig. 18 shows the output data planes (i.e., the $\mathcal{D}_p(\boldsymbol{\theta})$ in (39) for the JDL-UCR, the $\mathcal{Z}_p(\boldsymbol{\theta})$ in (65) for the JDL-RCM or JDL-ECM, and $p = 1, 2, 3$) at the 416-th frame produced by all of the algorithms. We can see that Target C is miss detected by the JDL-RCM algorithm due to a false alarm occurring. However, the JDL-ECM keeps robustness to detect and localize as it reserves the echoes of Target C from Radar 2, 3 and 4, then

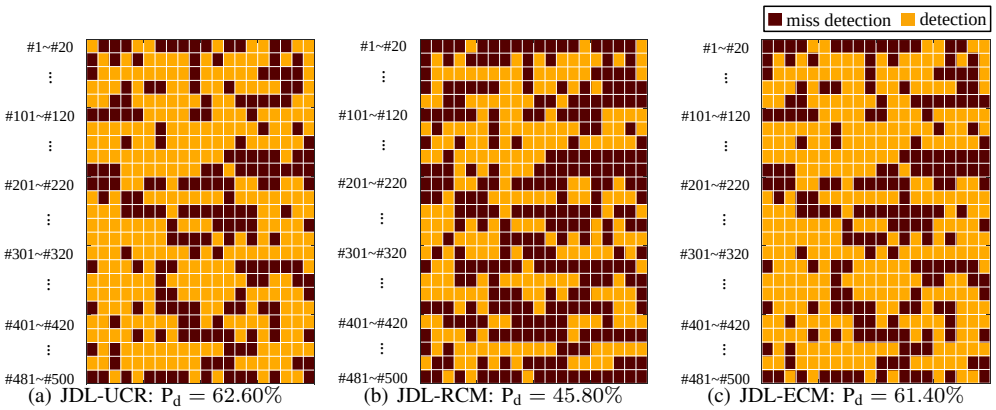

(a) JDL-UCR: $P_d = 62.60\%$ (b) JDL-RCM: $P_d = 45.80\%$ (c) JDL-ECM: $P_d = 61.40\%$

Figure 16. The detection results of 500 frames (organized into 25 rows and 20 columns) of the Scenario 1 with Target B are presented. Here, the brown and orange squares represent miss detection and detection, respectively. Each square symbolizes the detection outcome of a frame, with the left numbers indicating frame indices. The subfigures (a)–(c) respectively depict the results for the JDL-UCR, JDL-RCM, and JDL-ECM algorithms.

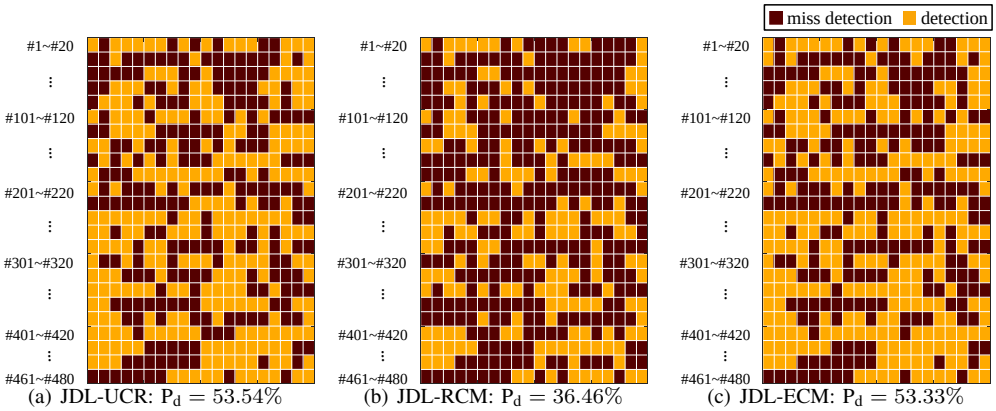

(a) JDL-UCR: $P_d = 53.54\%$ (b) JDL-RCM: $P_d = 36.46\%$ (c) JDL-ECM: $P_d = 53.33\%$

Figure 17. The detection results of 480 frames (organized into 24 rows and 20 columns) of the Scenario 2 with Target C, where the subfigures (a)–(c) denote the results for the JDL-UCR, JDL-RCM, and JDL-ECM algorithms, respectively.

achieving a higher-SNR data fusion under the same limited communication rates.

VI. Conclusions

In this paper, we have addressed the problem of JDL for distributed monopulse radars under communication constraints. We devised the JDL-UCR algorithm which utilizes complete LLR values to systematically detect and localize multiple targets one after another through iterative processes. While the JDL-UCR achieves superior performance, it demands high data transmission rates that can be impractical in wireless communication-constrained environments. To limit communication costs, we proposed the JDL-ECM algorithm, utilizing regular censoring and data updating steps, which effectively excludes the non-essential data and filters the informative data thus maintaining high performance. Finally, comprehensive simulation and real data analyses have been provided to demonstrate the effectiveness of our proposed algorithm, where high detection and localization performance is still guaranteed in the stringent communication constraints. Future works may consider the cases of non-line-of-sight (NLoS) or cooperative-communicating targets; distributed radars with partial/no knowledge of the noise covariance matrices; the refining of experimental measurements by exploring more controlled scenarios; and finally, the JDL of multiple moving targets in distributed multi-pulse radar systems with limited communication rates, incorporating the association of small parts of Doppler-dimensional data from local radars.

Appendix A
Proof of Proposition 1

Firstly, we define the $L_n^{(k)}[m]$ located at the m-th delay bin of the original LLR data $\mathbf{L}_n^{(k)}$ as y, which is expressed as

$$y = L_n^{(k)}[m] = \frac{\left|\mathbf{s}_n^H(\tau_n^m)\mathbf{R}_n^{-1}\mathbf{r}_n^{(k)}\right|^2}{\mathbf{s}_n^H(\tau_n^m)\mathbf{R}_n^{-1}\mathbf{s}_n(\tau_n^m)} \tag{72}$$

where $y \geq 0$ and $\tau_n^m = mT_s$ for $m = 1, 2, \ldots, M$ and $n = 1, \ldots, N$. Given the thumbtack auto-correlation assumptions of waveforms and the known noise covariance $\mathbf{R}_n = \sigma_w^2\mathbf{I}_M$, y can be further computed as

$$y = \left|\mathbf{w}_n^{(k)}[m]\right|^2 / \sigma_w^2 \tag{73}$$

under hypothesis $\mathcal{H}_0^{'}$, and as

$$y = \left|\alpha_{n,p} + \mathbf{w}_n^{(k)}[m]\right|^2 / \sigma_w^2 \tag{74}$$

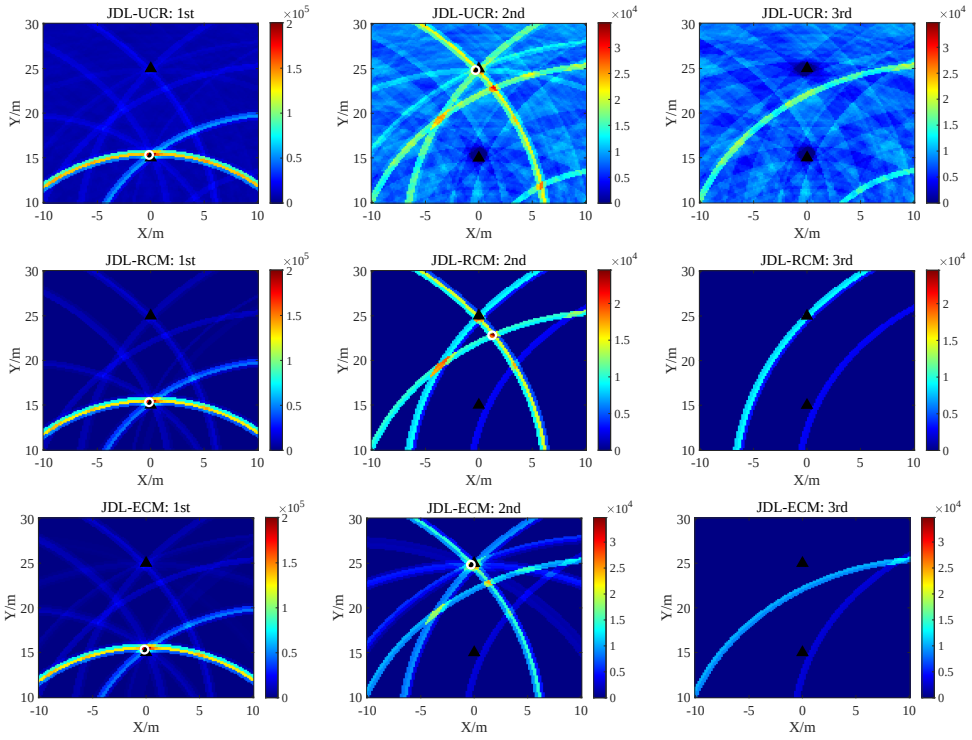

Figure 18. Output data planes of different algorithms (the $\mathcal{D}_p(\boldsymbol{\theta})$ in (39) for the JDL-UCR(top), the $\mathcal{Z}_p(\boldsymbol{\theta})$ in (65) for the JDL-RCM (middle) or JDL-ECM (bottom), and $p = 1, 2, 3$) in three consecutive iterations (from left to right) at the 416-th frame of Scenario 2, where the triangle markers are the true target positions (the above one is Target C, the other one is Target D), and the circle marker is the estimated position of the target detected (if any) at each iteration. We can see the JDL-UCR and JDL-ECM succeed in detecting and localizing both of the two targets, while JDL-RCM failed to detect Target C.

under hypothesis $\mathcal{H}_1^{'}$, where $\mathcal{H}_0^{'}$ denotes the hypothesis that no target is present at the m-th delay bin, i.e., $\tau_n^m \neq \tau_n(\boldsymbol{\theta}_p), \forall p$. Conversely, $\mathcal{H}_1^{'}$ denotes the hypothesis that the p-th target ($p = 1, \dots P$) is located at the m-th delay bin, i.e., $\tau_n^m = \tau_n(\boldsymbol{\theta}_p)$. Since $\mathbf{w}_n^{(k)}[m] \sim \mathcal{CN}\left(0, \sigma_w^2\right)$, the variable y follows the exponential distribution with parameter 1 under $\mathcal{H}_0^{'}$ and a non-central chi-square distribution with 2 degrees of freedom and non-centrality parameter $|\alpha_{n,p}|^2/\sigma_w^2$ under $\mathcal{H}_1^{'}$ [69]. The PDFs under the $\mathcal{H}_0^{'}$ and $\mathcal{H}_1^{'}$ are, respectively:

$$\mathrm{p}(y|\mathcal{H}_0^{'}) = e^{-y}, \tag{75}$$

and

$$\mathrm{p}(y|\mathcal{H}_1^{'}) = e^{(-y-\frac{|\alpha_{n,p}|^2}{\sigma_w^2})}\mathcal{I}_0\left(2\sqrt{\frac{|\alpha_{n,p}|^2}{\sigma_w^2}y}\right), \tag{76}$$

where $\mathcal{I}_0$ is the modified Bessel function of the first kind of order zero.

As mentioned in Remark 6, the given data retaining percentage $\mathrm{P}_{\mathrm{re},n}$ is treated as the local false alarm probability. This can be interpreted as the probability that y exceeds the detection threshold $\rho_{n,m}^{(k)}$ under $\mathcal{H}_0^{'}$. Mathematically, this is expressed as

$$\begin{aligned}\mathrm{P}_{\mathrm{re},n} &= \Pr(y > \rho_{n,m}^{(k)}|\mathcal{H}_0^{'}) \\ &= \int_{\rho_{n,m}^{(k)}}^{\infty} \mathrm{p}(y|\mathcal{H}_0^{'})\, d(y) \\ &= e^{-\rho_{n,m}^{(k)}}\end{aligned} \tag{77}$$

Then the closed-form detection threshold is determined by

$$\rho_{n,m}^{(k)} = -\ln \mathrm{P}_{\mathrm{re},n}, \tag{78}$$

which is also the desired censoring threshold. Consequently, Proposition 1 is proved.

Appendix B
Proof of Proposition 2

Here we aim to obtain the adaptive censoring thresholds by employing the CA-CFAR detection method, based on the original LLR data $\mathbf{L}_n^{(k)}$, data retaining percentage $\mathrm{P}_{\mathrm{re},n}$, and the assumed number of one-sided adjacent reference cells D. As mentioned in Remark 6, $\mathrm{P}_{\mathrm{re},n}$ is treated as the local false alarm probability.

Following the basic theory of CA-CFAR detection with square-law detector in [64], we employ $2D$ adjacent cells around the detection cell $L_n^{(k)}[m]$ to estimate the corresponding interference power $\hat{\sigma}_{k,n}^2[m]$ by averaging the squared modulus values of adjacent $2D$ cells, i.e.,

$$\hat{\sigma}_{k,n}^2[m] = \frac{1}{2D}\sum_{d=1}^{D}\left(\left|L_n^{(k)}[m-d]\right|^2 + \left|L_n^{(k)}[m+d]\right|^2\right) \tag{79}$$

for $m = 1, 2, \dots, M$ and $n = 1, \dots, N$. Also, given the local false alarm probability $\mathrm{P}_{\mathrm{re},n}$, the required threshold multiplier derived in the CA-CFAR basic theory can be directly calculated by [64, eq. (7.17)]

$$\beta_n = 2D(\mathrm{P}_{\mathrm{re},n}^{-\frac{1}{2D}} - 1). \tag{80}$$

Multiplying (79) and (80) and taking the square root, the adaptive detection thresholds can be determined by

$$\begin{aligned}\rho_{n,m}^{(k)} &= \sqrt{\hat{\sigma}_{k,n}^2[m]\beta_n} \\ &= \sqrt{(\mathrm{P}_{\mathrm{re},n}^{-\frac{1}{2D}} - 1)\sum_{d=1}^{D}(\left|L_n^{(k)}[m-d]\right|^2 + \left|L_n^{(k)}[m+d]\right|^2)},\end{aligned} \tag{81}$$

which is also the desired adaptive censoring threshold. Consequently, Proposition 2 is proved.

REFERENCES

[1] C. Baker and A. Hume, "Netted radar sensing," *IEEE Aerospace and Electronic Systems Magazine*, vol. 18, no. 2, pp. 3–6, 2003.

[2] H. Nikookar, "Signal design for context aware distributed radar sensing networks based on wavelets," *IEEE Journal of Selected Topics in Signal Processing*, vol. 9, no. 2, pp. 204–215, 2014.

[3] W. Yi, Y. Yuan, R. Hoseinnezhad, and L. Kong, "Resource scheduling for distributed multi-target tracking in netted colocated mimo radar systems," *IEEE Transactions on Signal Processing*, vol. 68, pp. 1602–1617, 2020.

[4] W. Yi, Y. Yuan, G. Liu, J. Ge, L. Kong, and J. Yang, "Recent advances in multi-radar collaborative surveillance: Cognitive tracking and resource scheduling algorithms," *Journal of Radars*, vol. 12, no. 3, pp. 471–499, 2023.

[5] C. Yang, W. Yi, and B. Champagne, "Joint antenna selection and beamforming for area surveillance with spatially distributed array radar," *IEEE Transactions on Aerospace and Electronic Systems*, vol. 61, no. 2, pp. 2899–2913, 2025.

[6] J. Wang, "CFAR-based interference mitigation for FMCW automotive radar systems," *IEEE Transactions on Intelligent Transportation Systems*, vol. 23, no. 8, pp. 12 229–12 238, 2021.

[7] S. Waqar, M. Muaaz, and M. Pätzold, "Direction-independent human activity recognition using a distributed MIMO radar system and deep learning," *IEEE Sensors Journal*, vol. 23, no. 20, pp. 24 916–24 929, 2023.

[8] E. Fishler, A. Haimovich, R. S. Blum, L. J. Cimini, D. Chizhik, and R. A. Valenzuela, "Spatial diversity in radars—models and detection performance," *IEEE Transactions on Signal Processing*, vol. 54, no. 3, pp. 823–838, Feb. 2006.

[9] Q. He and R. S. Blum, "Diversity gain for MIMO neyman–pearson signal detection," *IEEE Transactions on Signal Processing*, vol. 59, no. 3, pp. 869–881, 2010.

[10] L. Wang, M. Cheney, and B. Borden, "Multistatic radar imaging of moving targets," *IEEE Transactions on Aerospace and Electronic Systems*, vol. 48, no. 1, pp. 230–242, 2012.

[11] J. Liu, H. Li, and B. Himed, "Persymmetric adaptive target detection with distributed MIMO radar," *IEEE Transactions on Aerospace and Electronic Systems*, vol. 51, no. 1, pp. 372–382, 2015.

[12] S. Yang, A. Jakobsson, and W. Yi, "Moving target detection using a distributed MIMO radar system with synchronization errors," *IEEE Transactions on Geoscience and Remote Sensing*, vol. 61, pp. 1–17, 2023.

[13] N. H. Nguyen and K. Doğançay, "Optimal geometry analysis for multistatic TOA localization," *IEEE Transactions on Signal Processing*, vol. 64, no. 16, pp. 4180–4193, 2016.

[14] R. Xie, K. Luo, and T. Jiang, "Joint coverage and localization driven receiver placement in distributed passive radar," *IEEE Transactions on Geoscience and Remote Sensing*, vol. 59, no. 2, pp. 1094–1105, 2020.

[15] J. Sun, W. Yi, P. K. Varshney, and L. Kong, "Resource scheduling for multi-target tracking in multi-radar systems with imperfect detection," *IEEE Transactions on Signal Processing*, vol. 70, pp. 3878–3893, 2022.

[16] S. Nayemuzzaman, K. V. Mishra, and M. Saquib, "Multi-target tracking for full-duplex distributed integrated sensing and communications," in *2023 57th Asilomar Conference on Signals, Systems, and Computers*. IEEE, 2023, pp. 1673–1678.

[17] S. Nayemuzzaman, K. V. Mishra, J. Liu, and M. Saquib, "Co-designing statistical MIMO radar and in-band full-duplex multi-user MIMO communications–part III: Multi-target tracking," *arXiv preprint arXiv:2403.19120*, 2024.

[18] H.-J. Shao, X.-P. Zhang, and Z. Wang, "Efficient closed-form algorithms for AOA based self-localization of sensor nodes using auxiliary variables," *IEEE Transactions on Signal Processing*, vol. 62, no. 10, pp. 2580–2594, 2014.

[19] S. Zhao, X.-P. Zhang, X. Cui, and M. Lu, "Optimal two-way TOA localization and synchronization for moving user devices with clock drift," *IEEE Transactions on Vehicular Technology*, vol. 70, no. 8, pp. 7778–7789, 2021.

[20] S. Zhou and H. Liu, "Signal fusion-based target detection algorithm for spatial diversity radar," *IET Radar, Sonar Navigation*, vol. 5, no. 3, pp. 204–214, Mar. 2011.

[21] P. K. Varshney, *Distributed detection and data fusion*. Springer Science & Business Media, 2012.

[22] R. Amiri, F. Behnia, and M. A. M. Sadr, "Exact solution for elliptic localization in distributed MIMO radar systems," *IEEE Transactions on Vehicular Technology*, vol. 67, no. 2, pp. 1075–1086, Oct. 2017.

[23] Q. He, N. H. Lehmann, R. S. Blum, and A. M. Haimovich, "MIMO radar moving target detection in homogeneous clutter," *IEEE Transactions on Aerospace and Electronic Systems*, vol. 46, no. 3, pp. 1290–1301, Jul. 2010.

[24] P. Wang and H. Li, "Target detection with imperfect waveform separation in distributed MIMO radar," *IEEE Transactions on Signal Processing*, vol. 68, pp. 793–807, Jan. 2020.

[25] Y. Lai, G. Zhang, S. Yang, W. Yi, and L. Kong, "A quantization based censoring detection method with limited communication rates for distributed mimo radar," in *2021 CIE International Conference on Radar (Radar)*. IEEE, 2021, pp. 1188–1191.

[26] S. Yang, W. Yi, and A. Jakobsson, "Multitarget detection strategy for distributed MIMO radar with widely separated antennas," *IEEE Transactions on Geoscience and Remote Sensing*, vol. 60, pp. 1–16, 2022.

[27] Q. He, R. S. Blum, and A. M. Haimovich, "Noncoherent MIMO radar for location and velocity estimation: More antennas means better performance," *IEEE Transactions on Signal Processing*, vol. 58, no. 7, pp. 3661–3680, Mar. 2010.

[28] H. Godrich, A. M. Haimovich, and R. S. Blum, "Target localization accuracy gain in MIMO radar-based systems," *IEEE Transactions on Information Theory*, vol. 56, no. 6, pp. 2783–2803, May 2010.

[29] O. Bar-Shalom and A. J. Weiss, "Direct positioning of stationary targets using MIMO radar," *Signal Processing*, vol. 91, no. 10, pp. 2345–2358, Oct. 2011.

[30] R. Niu, R. S. Blum, P. K. Varshney, and A. L. Drozd, "Target localization and tracking in noncoherent multiple-input multiple-output radar systems," *IEEE Transactions on Aerospace and Electronic Systems*, vol. 48, no. 2, pp. 1466–1489, 2012.

[31] G. Zhang, W. Yi, P. K. Varshney, and L. Kong, "Direct target localization with quantized measurements in noncoherent distributed MIMO radar systems," *IEEE Transactions on Geoscience and Remote Sensing*, vol. 61, pp. 1–18, 2023.

[32] Q. Zhou *et al.*, "Target localization for distributed hybrid active-passive radars," *IEEE Transactions on Aerospace and Electronic Systems*, 2025, doi: 10.1109/TAES.2024.3483785.

[33] A. Tajer, G. H. Jajamovich, X. Wang, and G. V. Moustakides, "Optimal joint target detection and parameter estimation by MIMO radar," *IEEE Journal of Selected Topics in Signal Processing*, vol. 4, no. 1, pp. 127–145, 2010.

[34] G. V. Moustakides, G. H. Jajamovich, A. Tajer, and X. Wang, "Joint detection and estimation: Optimum tests and applications," *IEEE Transactions on Information Theory*, vol. 58, no. 7, pp. 4215–4229, 2012.

[35] W. Yi, T. Zhou, Y. Ai, and R. S. Blum, "Suboptimal low complexity joint multi-target detection and localization for non-coherent MIMO radar with widely separated antennas," *IEEE Transactions on Signal Processing*, vol. 68, pp. 901–916, 2020.

[36] Y. Lai, L. Venturino, E. Grossi, and W. Yi, "Joint detection and localization in distributed MIMO radars employing waveforms with imperfect auto- and cross-correlation," *IEEE Transactions on Vehicular Technology*, vol. 72, no. 12, pp. 16 524–16 537, 2023.

[37] L. Zhu, G. Wen, Y. Liang, D. Luo, and H. Song, "Energy-guided multitarget detection and localization for distributed MIMO radar: Analysis and solution," *IEEE Transactions on Aerospace and Electronic Systems*, vol. 59, no. 1, pp. 82–97, 2022.

[38] L. Zhu, G. Wen, Y. Liang, D. Luo, and H. Jian, "Multitarget enumeration and localization in distributed MIMO radar based on energy modeling and compressive sensing," *IEEE Transactions on Aerospace and Electronic Systems*, vol. 59, no. 4, pp. 4493–4510, 2023.

[39] Y. Lai, W. Yi, H. Wymeersch, M. F. Keskin, Q. Zhou, and L. Kong, "Joint detection and localization of multiple moving targets in a distributed radar system," *IEEE Sensors Journal*, vol. 24, no. 17, pp. 27 914–27 925, 2024.

[40] S. Gogineni and A. Nehorai, "Target estimation using sparse modeling for distributed MIMO radar," *IEEE Transactions on Signal Processing*, vol. 59, no. 11, pp. 5315–5325, 2011.

[41] B. Li and A. P. Petropulu, "Distributed MIMO radar based on sparse sensing: Analysis and efficient implementation," *IEEE Transactions on Aerospace and Electronic Systems*, vol. 51, no. 4, pp. 3055–3070, 2015.

[42] J. Liu, F. Lian, and M. Mallick, "Distributed compressed sensing based joint detection and tracking for multistatic radar system," *Information Sciences*, vol. 369, pp. 100–118, 2016.

[43] C. Li, G. Li, and P. K. Varshney, "Distributed detection of sparse stochastic signals with 1-bit data in tree-structured sensor networks," *IEEE Transactions on Signal Processing*, vol. 68, pp. 2963–2976, 2020.

[44] Z. Wang, Q. He, and R. S. Blum, "Target detection using quantized cloud MIMO radar measurements," *IEEE Transactions on Signal Processing*, vol. 70, pp. 1–16, 2021.

[45] M. Deng, Z. Cheng, L. Wu, B. Shankar, and Z. He, "One-bit ADCs/DACs based MIMO radar: Performance analysis and joint design," *IEEE Transactions on Signal Processing*, vol. 70, pp. 2609–2624, 2022.

[46] S. Yang, Y. Lai, A. Jakobsson, and W. Yi, "Hybrid quantized signal detection with a bandwidth-constrained distributed radar system," *IEEE Transactions on Aerospace and Electronic Systems*, vol. 59, no. 6, pp. 7835–7850, 2023.

[47] C. Rago, P. Willett, and Y. Bar-Shalom, "Censoring sensors: a low-communication-rate scheme for distributed detection," *IEEE Transactions on Aerospace and Electronic Systems*, vol. 32, no. 2, pp. 554–568, Apr. 1996.

[48] S. Appadwedula, V. V. Veeravalli, and D. L. Jones, "Decentralized detection with censoring sensors," *IEEE Transactions on Signal Processing*, vol. 56, no. 4, pp. 1362–1373, 2008.

[49] H. He and P. K. Varshney, "Fusing censored dependent data for distributed detection," *IEEE Transactions on Signal Processing*, vol. 63, no. 16, pp. 4385–4395, 2015.

[50] A. Mohammadi, S. H. Javadi, D. Ciuonzo, V. Persico, and A. Pescapè, "Distributed detection with fuzzy censoring sensors in the presence of noise uncertainty," *Neurocomputing*, vol. 351, pp. 196–204, 2019.

[51] Q. Hu, H. Su, S. Zhou, Z. Liu, Y. Yang, and J. Liu, "Two-stage constant false alarm rate detection for distributed multiple-input–multiple-output radar," *IET Radar, Sonar Navigation*, vol. 10, no. 2, pp. 264–271, Feb. 2016.

[52] D. Cao, S. Zhou, H. Liu, J. Liu, and H. Zang, "Signal censoring and fusing with system-level communication constraints in multistatic radar: a J-divergence and Bhattacharyya distance-based approach," *IET Radar, Sonar & Navigation*, vol. 11, no. 12, pp. 1802–1814, 2017.

[53] C. Li, G. Li, and P. K. Varshney, "Distributed detection of sparse signals with censoring sensors in clustered sensor networks," *Information Fusion*, vol. 83, pp. 1–18, 2022.

[54] D. Orlando and G. Ricci, "Adaptive radar detection and localization of a point-like target," *IEEE Transactions on Signal Processing*, vol. 59, no. 9, pp. 4086–4096, 2011.

[55] M. I. Skolnik, *Radar handbook*. 3rd ed. New York: Tata McGraw-Hill, 2008.

[56] Q. He, R. S. Blum, H. Godrich, and A. M. Haimovich, "Target velocity estimation and antenna placement for MIMO radar with widely separated antennas," *IEEE Journal of Selected Topics in Signal Processing*, vol. 4, no. 1, pp. 79–100, 2010.

[57] Z. Yu, J. Li, Q. Guo, and J. Ding, "Efficient direct target localization for distributed MIMO radar with expectation propagation and belief propagation," *IEEE Transactions on Signal Processing*, vol. 69, pp. 4055–4068, 2021.

[58] W. Liu, J. Liu, H. Li, Q. Du, and Y.-L. Wang, "Multichannel signal detection based on wald test in subspace interference and gaussian noise," *IEEE Transactions on Aerospace and Electronic Systems*, vol. 55, no. 3, pp. 1370–1381, 2018.

[59] J. Liu, Z.-J. Zhang, Y. Cao, and S. Yang, "A closed-form expression for false alarm rate of adaptive MIMO-GLRT detector with distributed MIMO radar," *Signal Processing*, vol. 93, no. 9, pp. 2771–2776, 2013.

[60] S. Chao, B. Chen, and C. Li, "Grid cell based detection strategy for MIMO radar with widely separated subarrays," *AEU-International Journal of Electronics and Communications*, vol. 66, no. 9, pp. 741–751, 2012.

[61] H. L. Trees, *Detection, Estimation, and Modulation Theory: Part III. Radar-sonar Signal Processing and Gaussian Signal in Noise*. John Wiley & Sons, Incorporated, 2001.

[62] P. Stoica and Y. Selen, "Model-order selection: a review of information criterion rules," *IEEE Signal Processing Magazine*, vol. 21, no. 4, pp. 36–47, Jul. 2004.

[63] P. Stoica, Y. Selen, and J. Li, "On information criteria and the generalized likelihood ratio test of model order selection," *IEEE Signal Processing Letters*, vol. 11, no. 10, pp. 794–797, Oct. 2004.

[64] M. A. Richards, *Fundamentals of radar signal processing*. Mcgraw-hill New York, 2005, vol. 1.

[65] H. W. Kuhn, "The hungarian method for the assignment problem," *Naval research logistics quarterly*, vol. 2, no. 1-2, pp. 83–97, 1955.

[66] C. Aydogdu *et al.*, "Radar interference mitigation for automated driving: Exploring proactive strategies," *IEEE Signal Processing Magazine*, vol. 37, no. 4, pp. 72–84, 2020.

[67] A. De Maio and M. Lops, "Design principles of MIMO radar detectors," *IEEE Transactions on Aerospace and Electronic Systems*, vol. 43, no. 3, pp. 886–898, 2007.

[68] J. Stastny, S. Cheung, G. Wiafe, K. Agyekum, and H. Greidanus, "Application of RADAR corner reflectors for the detection of small vessels in synthetic aperture radar," *IEEE Journal of Selected Topics in Applied Earth Observations and Remote Sensing*, vol. 8, no. 3, pp. 1099–1107, 2014.

[69] S. Papoulis, *Probability, Random Variables and Stochastic Processes by Athanasios*. Boston: McGraw-Hill, 2002.

Yangming Lai (Member, IEEE) received the B.E. and Ph.D. degrees in information and communication engineering from the University of Electronic Science and Technology of China, Chengdu, China, in 2018 and 2024, respectively. Since 2024, he has been an Associate Professor of the Department of Electronic Information Engineering with the School of Advanced Manufacturing, Fuzhou University, China. From October 2022 to October 2023, he was a Visiting Ph.D. Student with the Communication Systems Group, Department of Electrical Engineering, Chalmers University of Technology, Gothenburg, Sweden, under the financial support from the China Scholarship Council. His research interests include statistical signal processing, radar signal processing, and joint radar-communications, especially target detection and localization technologies.

Shixing Yang (Member, IEEE) received his B.E. degree in Electronic Information Engineering from Harbin Engineering University and his Ph.D. in Information and Communication Engineering processing from University of Electronic Science and Technology of China in 2017 and 2023, respectively. From 2021 to 2022, he was a visiting student at the Mathematical Statistics with Lund University, Sweden. He is currently a Tenure-track Associate Professor with the National Key Laboratory of Radar Signal Processing, Xidian University from 2024. His research interests include statistical signal processing, distributed radar signal processing, and MIMO radar detection technology.

Musa Furkan Keskin (Member, IEEE) received the Ph.D. degree in Electrical and Electronics Engineering from Bilkent University, Ankara, Turkey, in 2018. He is currently a Research Specialist in the Department of Electrical Engineering at Chalmers University of Technology in Gothenburg, Sweden, where he is leading and contributing to various interdisciplinary and industry-focused research projects at both Swedish and European levels, with a specialization in integrated localization, communication and sensing in 6G systems. His awards include the 2019 IEEE Turkey Best Ph.D. Thesis Award for his work on visible light positioning systems, the EU MSCA Postdoctoral Fellowship for his project "OTFS-RADCOM: A New Waveform for Joint Radar and Communications Beyond 5G.", and, the Swedish Research Council (VR) Starting Grant for his project on “Localization and Sensing for Perceptive Cell-Free Networks Towards 6G”. Dr. Keskin serves as an Editor for the IEEE Transactions on Communications and IEEE Transactions on Mobile Computing.

Henk Wymeersch (Fellow, IEEE) obtained the Ph.D. degree in Electrical Engineering/Applied Sciences in 2005 from Ghent University, Belgium. He is currently a Professor of Communication Systems with the Department of Electrical Engineering at Chalmers University of Technology, Sweden. Prior to joining Chalmers, he was a postdoctoral researcher from 2005 until 2009 with the Laboratory for Information and Decision Systems at the Massachusetts Institute of Technology. Prof. Wymeersch served as Associate Editor for IEEE Communication Letters, IEEE Transactions on Wireless Communications, and IEEE Transactions on Communications and is currently Senior Member of the IEEE Signal Processing Magazine Editorial Board. During 2019-2021, he was an IEEE Distinguished Lecturer with the Vehicular Technology Society. His current research interests include the convergence of communication and sensing, in a 5G and Beyond 5G context.

Lingjiang Kong (Senior Member, IEEE) was born in 1974. He received the B.S. degree in electronic engineering and the M.S. and Ph.D. degrees in signal and information processing from the University of Electronic Science and Technology of China (UESTC), Chengdu, China, in 1997, 2000, and 2003, respectively. From September 2009 to March 2010, he was a Visiting Researcher with the University of Florida, Gainesville, FL, USA. He is currently a Professor with the School of Information and Communication Engineering, UESTC. His research interests include multiple-input multiple-output radar, through the wall radar, and statistical signal processing.

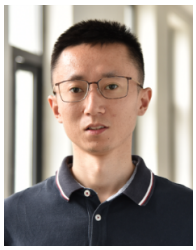

Wei Yi (Senior Member, IEEE) received the B.E. and Ph.D. degrees in electronic engineering from the University of Electronic Science and Technology of China, Chengdu, China, in 2006 and 2012, respectively. From 2010 to 2012, he was a Visiting Student with the Melbourne Systems Laboratory, University of Melbourne, Melbourne, VIC, Australia.

Since 2012, he has been with the University of Electronic Science and Technology of China, where he is currently a Full Professor with the School of Information and Communication Engineering. His research interests include target detection and tracking, radar signal processing, multi-sensor information fusion, and resources management.

Dr. Yi was the recipient of the Best Student Paper Competition-First place award at the 2012 IEEE Radar Conference, Atlanta, Best Student Paper Award at the 15th FUSION Conference, Singapore, 2012. He is the Associate Editor of IEEE Transactions of Signal Processing, IEEE Transactions on Aerospace and Electronic Systems, and a Member of the Editorial Boards of the Journal of Radars, the MDPI Sensors. He was also the General Co-Chair of ICCAIS 2019 and a Technical Program Committee Member of international conferences, such as IEEE Radar Conference and FUSION Conference.